= 1.3 Hz, 1 H), 10.88 (ds,[57] 2-phen*H*, $J_{2,3}$ = 5.5, J_{PtH} = 14.6 Hz, 1 H); IR (KBr) 1744 (C=O), 1129 (C—O), 847, 718 cm^{-1}. Anal. Calcd for $C_{22}H_{22}N_2Cl_2O_8Pt$: C, 37.30; H, 3.13; N, 3.95. Found: C, 37.42; H, 3.22, N, 3.76.

When method B was used with 16, the cis complex **21** was also isolated. ***cis*-Dichloro-*cis*(dimethyl malonato-*C*)(1,10-phenanthroline)platinum(IV) (21)**: 5%; mp >260 °C; ^1H NMR δ 2.56 (ss,[57] C*H*$_3$, J_{PtH} = 2.2 Hz, 3 H), 3.58 (ss,[57] C*H*$_3$, J_{PtH} = 2.5 Hz, 3 H), 3.73 (s, C*H*$_3$, J_{PtH} = 2.2 Hz, 3 H), 3.84 (s, C*H*$_3$, J_{PtH} = 2.2 Hz, 3 H), 4.52 (ss,[57] C*H*, J_{PtH} = 85.6 Hz, 1 H), 5.88 (ss,[57] C*H*, J_{PtH} = 98.9 Hz, 1 H), 7.92–8.16 (m, 3,5,6,8-phen*H*, 4 H), 8.59 (dd, 7-phen*H*, $J_{7,8}$ = 8.2, $J_{7,9}$ = 1.2 Hz, 1 H), 8.63 (dd, 4-phen*H*, $J_{3,4}$ = 8.3, $J_{2,4}$ = 1.3 Hz, 1 H), 9.60 (dds,[57] 2-phen*H*, $J_{2,3}$ = 5.4, $J_{2,4}$ = 1.3, J_{PtH} = 14.9 Hz, 1 H), 10.86 (dds,[57] 9-phen*H*, $J_{8,9}$ = 5.7, $J_{7,9}$ = 1.2, J_{PtH} = 30.4 Hz, 1 H) (insufficient sample for CHN analysis).

Attempt To Synthesize Pt(phen)(dmm)$_4$ (22). Dimethyl malonate (80 mg, 610 μmol) and anhydrous K_2CO_3 (134 mg, 970 μmol) were added to a solution of freshly prepared Pt(phen)(dmm)$_2$Br$_2$ (**18**) (75 mg, 90 μmol) in DMF (10 mL), and the solution was heated to 90 °C for 12 h. The DMF and excess malonate were then removed in vacuo, and the remaining solid was extracted with $CHCl_3$. After filtration and removal of the $CHCl_3$ the product was purified by flash-dry chromatography[56] eluting first with $CHCl_3$ and then with 30% MeOAc/$CHCl_3$.

The $CHCl_3$ fraction afforded (88%) **dimethyl 2,3-bis(methoxycarbonyl)butanedioate**,[58] as determined by ^1H NMR: 22 mg.

The MeOAc/$CHCl_3$ fraction afforded (77%) **bis(dimethyl malonato-*C*)(1,10-phenanthroline)platinum(II) (16)**: 47 mg.

Reaction of Pt(phen)(ddm)$_2$Br$_2$ (18) with NaOH. Pt(phen)(dmm)$_2$Br$_2$ (**18**) (40 mg, 50 μmol) in CH_2Cl_2 (5 mL) was added to a solution of NaOH (52 mg, 1.3 mmol) in EtOH (5 mL). The mixture was stirred for 15 min at 25 °C. More CH_2Cl_2 was added and the solution washed twice with aqueous saturated NaCl. The CH_2Cl_2 solution was then dried over anhydrous $MgSO_4$ and the solvent removed to give Pt(phen)(dmm)$_2$ (**16**) as a yellow solid (8 mg, 25%).

Acknowledgment. We wish to thank the National Science Foundation (CHE-15354), DOW Chemical, and the Engelhard Corp. for partial support of this research.

Supplementary Material Available: Listings of bond distances, bond angles, coordinates for H atoms, and anisotropic thermal parameters for **10a**, **10b**, and **11** (16 pages); listings of structure factor amplitudes for **10a**, **10b**, and **11** (70 pages). Ordering information is given on any current masthead page.

(58) Fronczek, F. R.; Gupta, V. K.; Newkome, G. R. *Acta Crystallogr.* 1983, *C39*, 1113.

Cooperative Effects in π-Ligand Bridged Binuclear Complexes. 8. Cyclic Voltammetric, NMR, and ESR Spectroscopic Studies of Electron-Poor Synfacial Bis($(\eta^5$-cyclopentadienyl)metal) μ-Cyclooctatetraene Complexes of Chromium and Vanadium

Bernd Bachmann, Friedemann Hahn, Jürgen Heck,* and Martin Wünsch

Fachbereich Chemie, Philipps-Universität Marburg, Hans-Meerwein-Strasse, 3550 Marburg, FRG

Received January 23, 1989

Electron-poor ($\sum$ve < 34) (ve = valence electron) synfacial μ-Cot (Cot = cyclooctatetraene) complexes of the general composition X(Cp'$_2$MM')(μ-Cot) (Cp' = C_5H_4; X = H,H, CH_2, $SiMe_2$, $GeMe_2$; M = M' = V, **1a–d**; M = M' = Cr, **2a–d**; M = V, M' = Cr, X = H,H, **3**) are studied by cyclic voltammetry and ESR as well as NMR spectroscopy. Except for (CpV)$_2$(μ-Cot) (**1a**) (Cp = C_5H_5) two electrochemically reversible redox pairs are found involving diffusion-controlled one-electron transfers: all compounds show a reduction step at −2 V (vs SCE) and in **2a–d** as well as in **3** an oxidation step occurs at about −0.7 V (vs SCE) whereas for **1b–d** the oxidation is not observed before E° > 0 V (vs SCE). A second electrochemically reversible redox pair, 1+/2+, is measured at E° > 0.3 V (vs SCE) for the dichromium complexes **2a–d**. All species within 28 ≤ $\sum$ve ≤ 31 are stable enough to be studied by NMR and ESR spectroscopy. The homobinuclear radical species with 29 and 31 ve contain an unpaired electron completely delocalized over both metal centers. In contrast to it, the unpaired electron in the mixed complex is localized on the V center mainly. From NMR spectroscopic results the 30 ve complexes are purely diamagnetic whereas the 28 ve compounds possess a low-lying triplet state (ΔH = 22–24 kJ mol^{-1}). This low-lying triplet state is explained by a qualitative MO diagram indicating only a small splitting between the HOMO (δMO) and LUMO (δ*MO). The ^1H NMR spectroscopic data confirm a strong diamagnetic anisotropy of the metal–metal multiple bond in **1a–d** ($\Delta\chi$ > 2000 × 10^{-36} m^3 $molecule^{-1}$) and **2a–d** ($\Delta\chi$ > 3000 × 10^{-36} m^3 $molecule^{-1}$).

Introduction

We reported the synthesis and structures as well as some magnetic properties of the homobinuclear μ-Cot complexes of the type (CpM)$_2$(μ-Cot) (M = V, **1a**; M = Cr, **2a**) in two recent papers.[2,3]

Two facts mainly prevail on us about getting more information on the metal–metal interaction in complexes of type **1a** and **2a**: (i) **1a** and **2a** have nearly the same structure and the intermetal distance in **1a** is about 5 pm longer than in **2a**, although the bond order in **1a** might be a triple bond, whereas the bond order in **2a** is a double bond with respect to the EAN rule and their magnetic

(1) Part 7, see ref 5. Part 6: Heck, J.; Kriebisch, K.-A.; Mellinghoff, H. *Chem. Ber.* 1988, *121*, 1753.

(2) (a) Elschenbroich, Ch.; Heck, J.; Massa, W.; Nun, E.; Schmidt, R. *J. Am. Chem. Soc.* 1983, *105*, 2905. (b) Heck, J.; Baltzer Ph.; Elschenbroich, Ch.; Massa, W.; Schmidt, R., Poster P13 on the 29th IUPAC Congress, Köln, 1983; Abstract p 81.

(3) (a) Elschenbroich, Ch.; Heck, J.; Massa, W.; Schmidt, R. *Angew. Chem.* 1983, *95*, 319. (b) Heck, J.; Rist, G. *J. Organomet. Chem.* 1988, *342*, 45.

0276-7333/89/2308-2523$01.50/0

Chart I

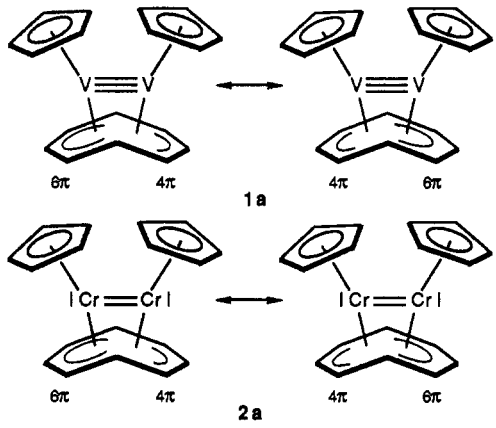

behavior at low temperature (Chart I); (ii) preliminary NMR studies of **1a** show line broadening and a downfield shift of the ^1H NMR signals upon increasing the temperature and the lack of some signals in the ^{13}C NMR spectrum at ambient temperature. These distinctive features let us assume that upon increasing the temperature an excited paramagnetic state will be populated in **1a**, whereas **2a** is purely diamagnetic.[2-4]

Therefore **1a** and **2a** seem to be interesting prototypes of compounds containing a M,M multiple bond, and we decided to perform an extended experimental study on these complexes as well as on some derivatives wherein the Cp ligands are linked via a bridging group, X (X = CH_2, $SiMe_2$, and $GeMe_2$). Because of the different sizes of the

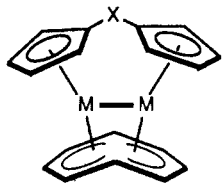

	X		
M	CH_2	$SiMe_2$	$GeMe_2$
V	**1b**	**1c**	**1d**
Cr	**2b**	**2c**	**2d**

bridging groups in the all-vanadium complexes (abbreviated as VV, **1a–d**) and in the all-chromium complexes (abbreviated as CrCr, **2a–d**), the metal–metal distances are somewhat different in these compounds.[4,5] Hence, some of their properties, such as the energy of the thermally excited paramagnetic state and the redox behavior as well as the ESR parameters of their radical species, might be influenced. In the course of our study on metal–metal interactions within this series of bimetallic μ-Cot complexes of the early transition metals, we also prepared the heterobimetallic compound $(Cp_2VCr)(\mu\text{-Cot})$ (abbreviated as VCr, **3**), an intermediate of the homobinuclear V and Cr species **1a** and **2a**, respectively. In contrast to VV and CrCr the mixed-metal compound VCr bears an odd number of electrons and hence will be paramagnetic.

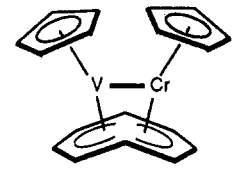

3

Experimental Section

All manipulations were carried out in a N_2 atmosphere and in N_2-saturated solvents. Tetrahydrofuran (THF), 2-methyltetrahydrofuran (MTHF), 1,2-dimethoxyethane (DME), and diethyl ether (Et_2O) were freshly distilled from the appropriate alkali metal or metal alloy/benzophenone; *n*-hexane was distilled from K/Na alloy, toluene from K, and acetone from K_2CO_3.

The electrochemical equipment was an Amel "Electrochemolab" (potentiostat, Model 552; function generator, Model 566; multifunction interface, Model 563) joined to a Nicolet storage oscilloscope (Model 2090-1) and a Kipp und Zonen X-Y recorder (Model BD 90). The reference electrode was an aqueous-saturated calomel electrode (SCE) and the auxiliary electrode a Pt wire. A glassy carbon electrode was used as a working electrode. The cyclic voltammetric measurements were carried out in DME and with 0.1 M tetra-*n*-butylammonium perchlorate (TBAP) as the supporting electrolyte, purchased from Fluka Feinchemikalien GmbH and purified by crystallization from absolute EtOH (1×) and DME (2×).

The ESR spectra were recorded on Varian EE 12 X-band and EE 15 Q-band spectrometers. The radical anions of the V and Cr complexes were generated in situ by contact of MTHF solutions of the complexes with potassium metal in a manner described previously.[6]

The ESR spectra of the Cr radical cation $\mathbf{2a}^{\bullet+}$ was once obtained from an electrochemical oxidation in an ESR cell (outer diameter 5 mm) equipped with a helical gold wire as the anode and an inner concentric Pt wire as the cathode. As it is not possible to join the definite potential obtained from the cyclic voltammetric measurement to this arrangement, the oxidation potential was successively enhanced until a radical could be observed ESR spectroscopically. A mixture of DME and THF (1/1) was used as the solvent with TBAP (0.5 M) as the supporting electrolyte.

The evidence that the observed resonance signal can indeed be derived from the electrochemically generated radical cation $\mathbf{2a}^{\bullet+}$ finally was performed by an additional study of an acetone solution of $\mathbf{2aPF_6}$, which was yielded chemically by $(FeCp_2)PF_6$ oxidation (vide infra). Additionally, identical ESR spectra could be obtained, if **2a** was allowed to react with 4-pyridinecarboxaldehyde in acetone. Therefore, the radical cations of the Cp-bridged derivatives of CrCr were studied in situ by oxidation of the neutral complexes with 4-pyridinecarboxaldehyde in acetone.

For the determination of the *g* values and calibration of the magnetic field Fremy's salt $ON(SO_3K)_2$ was used as the standard: $a(^{14}N) = 1.309$ mT; $g_{iso} = 2.005\,65$.

The NMR spectra of the neutral derivatives of the homobinuclear complexes VV and CrCr were obtained from $[^2H_8]$toluene solutions, whereas those of VCr^- were recorded after in situ reduction with potassium in $[^2H_8]$THF in an NMR tube. The NMR spectra of cations containing an even number of electrons were obtained from $[^2H_6]$acetone solutions. The spectra were recorded on a Bruker WH 400 spectrometer and in one case on a Varian T 60 spectrometer. The NMR tubes were sealed under vacuum.

The X-bridged compounds **1b–d** and **2b–d** were prepared quite similar to **1a** and **2a** in a one-pot reaction with the appropriate metal(II) chlorides, K_2Cot, and $Li_2[Cp'_2X]$.[2,3] A more detailed description is given elsewhere.[4,5] All compounds under investigation are extremely air-sensitive.

Preparation of $[(CpCr)_2(\mu\text{-Cot})]PF_6$ ($\mathbf{2aPF_6}$). **2a**[3] (150 mg, 0.44 mmol) and 140 mg (0.42 mmol) of $(FeCp_2)PF_6$ were stirred in 20 mL of acetone at −20 °C for 30 min. The dark green solution was filtered (G4) into a cooled flask (−20 °C), and 50 mL of Et_2O was added. The resulting green suspension was filtered off, and the microcrystalline green residue was washed with small portions of Et_2O and *n*-hexane. After being dried under vacuum, the crystalline solid was dissolved in 10 mL of acetone and treated with 30 mL of Et_2O. The green precipitate was isolated, washed

(4) Bachmann, B.; Baltzer, Ph.; Hahn, F.; Heck, J. Poster on the XIIth International Conference on Organometallic Chemistry, Wien, 1985; Abstract 250.

(5) Bachmann, B.; Heck, J.; Massa, W.; Ziegler, B. *Z. Naturforsch., B*, accepted for publication.

(6) Elschenbroich, Ch.; Bilger, E.; Heck, J.; Stohler, F.; Heinzer, J. *Chem. Ber.* **1984**, *117*, 23.

Table I. Cyclic Voltammetric Data[a] for the Binuclear μ-Cot Complexes X(Cp'$_2$MM')(μ-Cot) (1-3)

compounds		reductns −1/0		oxidatns 0/+1			oxidatns +1/+2			
		$E°$(red.)[b]	ΔE_p[c]	E°(ox.$_1$)[b]	ΔE_p[c]	$\Delta E°_1$[d]	E(ox.$_2$)[b,e]	ΔE_p[c]	$\Delta E°_2$[f]	T, °C
M = M' = V	X = H,H[g] (**1a**)	−2086 (5)	63	...	...		+319 (14) irrev	240	...	−36
	X = CH_2 (**1b**)	−2142 (6)	69	+17 (2))	75	2159 (8)	+369 (25) irrev	90	...	−37
	X = $SiMe_2$ (**1c**)	−2051 (1)	59	+87 (2)	59	2138 (3)	+443 (11) irrev	64	...	−36
	X = $GeMe_2$ (**1d**)	−2060 (2)	107	+73 (3)	76	2133 (5)	+336 (2) irrev	70	...	−38
M = M' = Cr	X = H,H (**2a**)	−2129 (2)	65	−703 (2)	66	1426 (4)	+430 (11) irrev[h]	100	...	+23
		−2110 (2)	176	−738 (1)	119	1372 (3)	+333 (2))	99	1071 (3)	−27
	X = CH_2 (**2b**)	−2176 (5)	105	−736 (2)	62	1440 (7)	+374 (4)	64	1110 (6)	+22
	X = $SiMe_2$ (**2c**)	−2097 (2)	58	−665 (2)	60	1432 (2)	+433 (6)	56	1098 (8)	+22
	X = $GeMe_2$ (**2d**)	−2101 (1)	81	−685 (1)	72	1416 (2)	+385 (2)	79	1070 (3)	+21
M = V, M' = Cr	X = H,H (**3**)	−2047 (2)	60	−653 (2)	60	1394 (4)	+556 (4) irrev[i]	60		+20

[a] Obtained from DME/0.1 M TBAP, glassy carbon, the potentials E and their differences ΔE are given in mV. [b] $E°$ values vs SCE. [c] $\Delta E_p = E_{pa} - E_{pc}$ for reversible and $\Delta E_p = E_{pa} - E_{pa/2}$ for irreversible processes, denoted as irrev. [d] $\Delta E°_1 = E°$(red.) − $E°$(ox.$_1$). [e] E(ox.$_2$) stands for E_{pa} in cases of irreversible and for $E°$ in cases of reversible oxidations, scan rate for irreversible processes: v = 100 mV/s. [f] $\Delta E°_2 = |E°(ox._1) - E°(ox._2)|$. [g] X = H,H stands for complexes without a bridge between the Cp ligands. [h] A third irreversible oxidation step is observed at E_p > 1600 mV. [i] An additional irreversible oxidation step is observed at E_p = +572 (10) mV at T = 20 °C.

with Et_2O and *n*-hexane, and dried under vacuum; yield: 80 mg (39%) of **2aPF$_6$**. Anal. Calcd for $C_{18}H_{18}Cr_2F_6P$: C, 44.73; H, 3.75. Found: C, 44.68; H, 4.09.

Preparation of (Cp$_2$VCr)(μ-Cot) (3). A solution of 340 mg (1,53 mmol) of CpCrCot (**4**)[7] in 20 mL of THF was poured into a flask containing 40 mL of a cooled THF solution (−40 °C) of $CpVCl_2$ (**5**) prepared from 330 mg (1.48 mmol) of $CpVCl_3$ and 200 mg (3.0 mmol) of activated Zn dust (see ref 8a). The reaction mixture was stirred overnight and allowed to warm to ambient temperature. The solution was restricted to 20 mL, and 20 mL of toluene was added to this solution. The dark red solution was filtered through a column of deactivated alumina (5% H_2O, 20 cm) and eluted with toluene until the eluate was colorless. The resulting deep red eluate was evaporated to dryness. The residue was dissolved in hot hexane for crystallization. After the solution was stored at −30 °C for 3 days, dark red-brown crystal could be obtained; yield 180 mg (37% based on **4**). **3** is moderately soluble in petroleum ether and well soluble in aromatic solvents and THF; fp 234 °C dec. Anal. Calcd for $C_{18}H_{18}CrV$: C, 64.10; H, 5.37; Cr, 15.42; V, 15.10. Found: C, 63.94; H, 5.53; Cr, 15.33; V, 15.23. IR (Nujol mull, CsI, cm^{-1}): 1220 w, 1115 w, 1005 m, 946 w, 928 w, 890 vw, 876 vw, 856 w, 840 vw, 828 sh, 805 s, 782 m, 762 w, 674 w, 518 w, 465 w, 440 w, 418 vw, 380 vw, 340 vw, 310 vw. EI-MS *m/e* (%) (only the mass peaks containing the main isotopes are taken into account): 337 (100) M^+, 233 (57.9) $(M - Cot)^+$, 221 (6.3) $(CpCrCot)^+$, 220 (11.3) $(CpVCot)^+$, 218 (33.9), 194 (11.1), 182 (58.1) $(CrCp_2)^+$, 181 (71.4) $(VCp_2)^+$, 153 (13.4), 117 (30.1) $(CpCr)^+$, 116 (72.8) $(VCp)^+$, 52 (84.1) Cr^+, 51 (14.3) V^+.

The oxidation of **3** to the monocation **3PF$_6$** was performed in the same manner as that of **2aPF$_6$**. A dark green microcrystalline powder was obtained; yield 79 mg (38.6%).

The preparation of the dication of the Cp-bridged Cr complex **2d** was attempted by oxidation with an excess of AgTFA (TFA = trifluoracetate) in acetone at −78 °C. The precipitated Ag was filtered off, and upon dilution with Et_2O, a dark brown solid was deposited, which is only partially soluble in acetone again. When an acetone solution of this solid was left standing in a refrigerator for a few days, a light green solution and a gray insoluble precipitate were formed.

Nevertheless, to perform a temperature ^1H NMR study of **2d^{2+}**, ca. 12 mg of **2d** was dissolved in [$^2H_6$]acetone in an NMR tube in the presence of ca. 30% excess of the required amount of $(Cp_2Fe)PF_6$. During the solvation the temperature was kept below −80 °C. At this temperature the NMR tube was stored until it was put into the NMR spectrometer, wherein it was allowed to warm up successively for the different measurements.

Results

Synthesis. The X-bridged compounds **1b–d** as well as **2b–d** were prepared in a one-pot reaction like **1a** and **2a** starting from the appropriate metal(II) chlorides, K_2Cot, and $Li_2(Cp'_2X)$[2-5] (eq 1).

$$2\text{"}MCl_2\text{"} + K_2Cot + Li_2(Cp'_2X) \rightarrow X(Cp'M)_2(\mu\text{-}Cot) \quad (1)$$

1b: M = V; X = CH_2
1c: M = V; X = $SiMe_2$
1d: M = V; X = $GeMe_2$
2b: M = Cr; X = CH_2
2c: M = Cr; X = $SiMe_2$
2d: M = Cr; X = $GeMe_2$

M = V: "MCl_2" = $\frac{1}{4}[V_2(\mu\text{-}Cl)_3(THF)_6]_2[Zn_2Cl_6]$[8b]

M = Cr: "MCl_2" = $\frac{1}{2}[CrCl_2(TMEDA)]_2$[3b]

The synthesis of the heterobinuclear complex **3** must be performed in a stepwise fashion. As a starting Cot complex we used the mononuclear sandwich compound (η^5-Cp)Cr(η^6-Cot) (**4**),[7] which possesses one uncoordinated carbon–carbon double bond predestined for further complexation.[3b,9]

The half-sandwich complex $CpVCl_2$ (**5**) was used[8] as a CpV unit for synthesizing **3**. Besides the opportunity of precoordination of the free double bond in **4** at the V center of **5**, the driving force for synthesizing **3** was enhanced by the formation of $ZnCl_2$ during reaction 2. The

$$\underset{\mathbf{4}}{CpCrCot} + \underset{\mathbf{5}}{CpVCl_2} \rightarrow \text{"}(CpCr)(CpVCl_2)(\mu\text{-}Cot)\text{"} \xrightarrow[-ZnCl_2]{Zn} \underset{\mathbf{3}}{(Cp_2VCr)(\mu\text{-}Cot)} \quad (2)$$

lack of any antifacial $(CpM)_2Cot$ species with M = Cr or V in the synthesis of **1a** and **2a** even if we tried to introduce bulky ligands like C_5Me_5 instead of Cp,[10] which are able to stabilize electron-poor metal centers in some cases,[11]

(7) Müller, J.; Menig, H. *J. Organomet. Chem.* **1975**, *96*, 83. **4** is also obtained as a byproduct in the synthesis of **2** (see ref 3b).

(8) (a) Thiele, K.-H.; Oswald, L. *Z. Anorg. Allg. Chem.* **1976**, *423*, 231. (b) Köhler, F. H.; Prössdorf, W. *Z. Naturforsch., B* **1977**, *32B*, 1026. (c) Bouma, J. R.; Teuben, J. H.; Beukema, W. R.; Bansemer, R. L.; Huffmann, J. C.; Caulton, K. G. *Inorg. Chem.* **1984**, *23*, 2715.

(9) The capability of the free double bond of the η^6-coordinated Cot ring in **4** to coordinate to a second metal center could be shown in our group: (η^5-C_5Me_5)Cr(η^6-Cot) + $CpMn(CO)_2(THF)$ → {[(η^5-C_5Me_5)Cr]-[(η^5-Cp)Mn(CO)$_2$]}(μ-η^6:η^2-Cot), Bachmann, B.; Heck, J., unpublished results.

(10) If in accord to the synthesis of **2a** the permethylated Cp anion $C_5Me_5^-$ was used instead of Cp^-, the only obtainable Cot complex was (η^5-C_5Me_5)Cr(η^6-Cot), the properties of which are very similar to those of (η^5-Cp)Cr(η^6-Cot) (see ref 3b). In contrast the use of V instead of Cr only results in the formation of the homoleptic complexes $V(C_5Me_5)_2$ and $V(Cot)_2$ (Bachmann, B. Diplomarbeit, Universität Marburg, 1985).

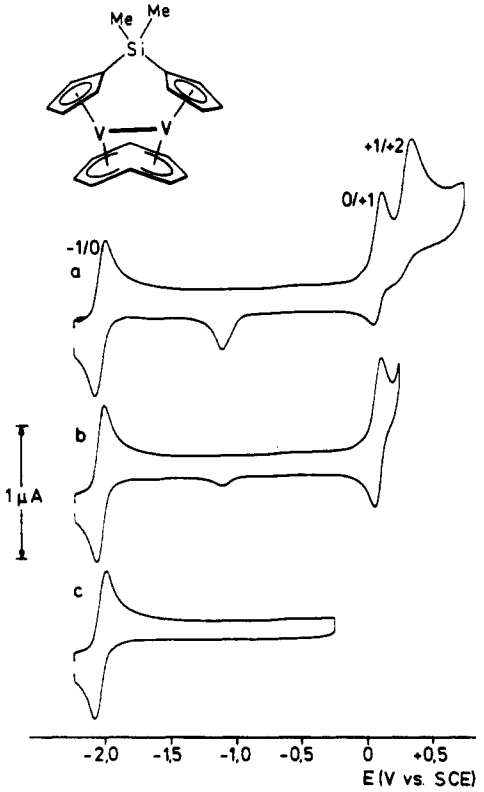

Figure 1. Typical cyclic voltammograms of Cp-linked divanadium compounds $X(Cp'V)_2(\mu\text{-Cot})$ illustrated for X = $SiMe_2$ (**1c**) (T = −36 °C).

reasonably points out that a very similar synfacial structure for VCr as well as for VV and CrCr can be taken for granted (vide supra). The spectroscopic properties of the paramagnetic complexes **3** are in accord with a synfacial structure (vide infra).

Redox Properties. The cyclic voltammetric data for **1–3** are listed in Table I. A typical cyclic voltammogram of the X-bridged VV complexes (X = $SiMe_2$) is depicted in Figure 1. It was recorded at T = −36 °C and contains two redox couples and one oxidation wave with diffusion-controlled electron transfers ($i_p \propto (v)^{1/2}$). The identical peak currents of the two redox couples and the irreversible oxidation indicate the same number of electrons involved in each redox process. The peak current ratio, i_{pa}/i_{pc} = 1.00 (5), of the two redox couples, which are attributed to a reduction for $E°$(red.) < −2 V and an oxidation for $E°(ox_1) > 0$ V, confirms their reversibility (see Figure 1b). A comparison of the peak separations, ΔE_p(−1/0;0/+1) ($\Delta E_p = |E_{pc} - E_{pa}|$), of the divanadium complexes **1b–d** with ΔE_p(0/+1) of bis(benzene)chromium as an internal standard[12,13] proves that the redox couples (−1/0) and (0/+1) of **1b–d** involve reversible one-electron transfers. This behavior agrees with the peak separations (ΔE_p) of 60–70 mV, which were obtained for several couples.[14]

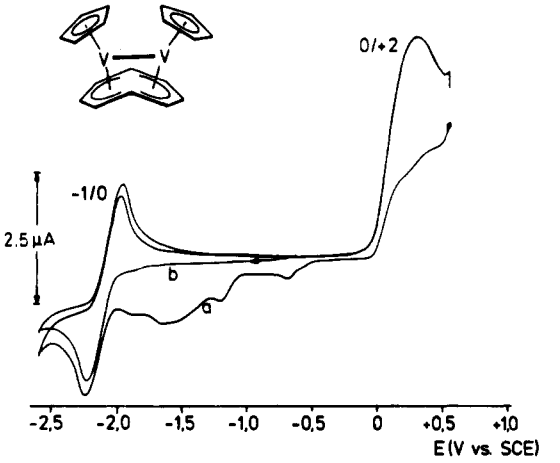

Figure 2. Cyclic voltammograms of $(CpV)_2(\mu\text{-Cot})$ (**1a**) (T = −36 °C).

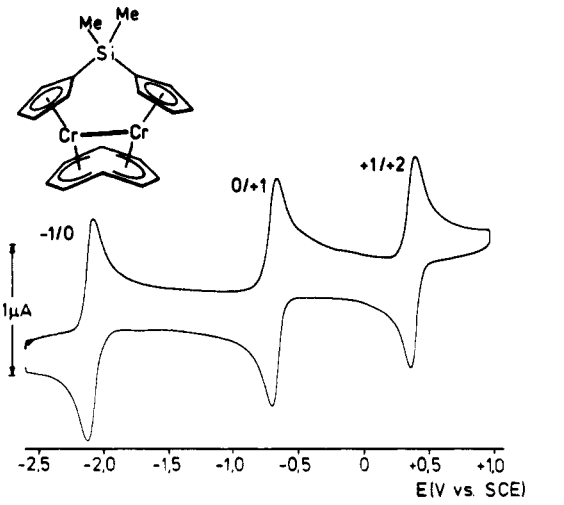

Figure 3. Typical cyclic voltammogram of Cp-linked dichromium compounds $X(Cp'Cr)_2(\mu\text{-Cot})$ illustrated for X = $SiMe_2$ (**2c**) (T = +22 °C).

As can be seen from Figure 1a–c, an extra reduction peak appears at E_{pc} < −1100 mV, which can only be observed when the potential of one cycle is about 160 mV more positive than the first oxidation potential ($E°(ox._1)$). Hence this reduction wave may be correlated with a species formed by the second, but irreversible oxidation. In contrast to the first oxidation of the Cp-bridged compounds **1b–d**, which is passably well separated from the second, irreversible one and is warranted at low temperature, only one broad irreversible oxidation peak can be observed for the parent complex **1a** even at low temperature (Figure 2). The peak current (i_{pa}) of 4.8 μA is nearly twice as large as i_{pa} of the reversible redox couple at $E°$(red.) = −2086 mV with i_{pa} = 2.3 μA, assuming two irreversible one-electron oxidations for **1a** (see Figure 2), which are close together and hence not resolved. The reversibility of the reduction step for **1a** can be shown by the ratio of i_{pa}/i_{pc} if the range of the cyclic voltammogram is chosen small enough as can be seen in Figure 2 (cycle b).

A more pronounced redox behavior was found for the corresponding Cr complexes **2a–d**. As an example, the cyclic voltammogram of **2c** (X = $SiMe_2$) is represented in Figure 3, showing three nicely separated redox couples attributing to one reduction step with $E°$(red.) < −2 V and two oxidation steps, $E°(ox._1)$ and $E°(ox._2)$. The peak separations (ΔE_p) as well as the peak currents (i_p) are almost identical for all three redox couples. The charge

(11) (a) Edwin, J.; Geiger, W. E.; Rheingold, A. L. *J. Am. Chem. Soc.* **1984**, *106*, 3052. (b) Calabro, D. C.; Hubbard, J. L.; Blevins II, C. H.; Campbell, A. C.; Lichtenberger, D. L. *J. Am. Chem. Soc.* **1981**, *103*, 6839 and references cited therein.

(12) A reversible one-electron oxidation has been established for **6** at $E°$ = −690 mV vs SCE (see ref 13).

(13) (a) Bilger, E.; Elschenbroich, Ch., private communication. See also: (b) Furlani, C.; Fischer, E. O. *Z. Electrochem.* **1957**, *61*, 481. Vlceck, A. A. *Z. Anorg. Allg. Chem.* **1960**, *304*, 109.

(14) The ΔE_p values are not always optimized; see Table I. The theoretical value of ΔE_p normally can be obtained, if freshly prepared electrolyte solvents and freshly cleaned electrodes are used.

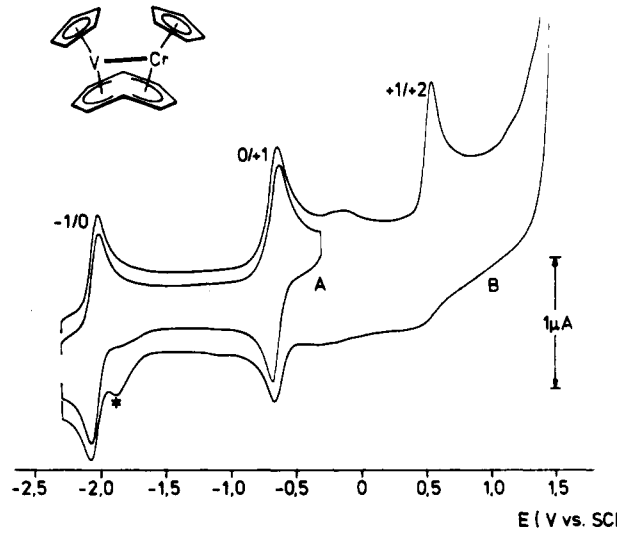

Figure 4. Cyclic voltammograms of $(Cp_2VCr)(\mu\text{-Cot})$ (**3**) (T = +20 °C) (for more information consult text).

transfers are diffusion-controlled, and unlike the corresponding VV species all three redox couples involve a reversible electron transfer as confirmed by the peak current ratios i_{pa}/i_{pc} = 1.00 (4). Only for **2a** the second oxidation step, $E°(ox._2)$, is irreversible at room temperature, but its reversibility has been shown at T = −27 °C. In several cases we obtained peak separations (ΔE_p) almost equal to 59 mV (see Table I).[14] Although this value already points to a one-electron transfer involved in each reversible redox couple, we used $Cr(C_6Me_6)_2$ (**7**) as an internal standard.[15] A comparison of ΔE_p for the redox couples of the binuclear Cr complexes with that of $7/7^+$ confirms that one electron is transferred in each step. The most striking evidence for a one-electron transfer involved in each redox couple of the all-chromium species was obtained from the cyclic voltammetric study of an analytically pure sample of the monocation $[(CpCr)_2(\mu\text{-Cot})]PF_6$ (**2aPF$_6$**), which revealed a cyclic voltammogram identical with that of the neutral compound **2a**.

Regarding the number of reversible redox couples of the dichromium as well as of the divanadium complexes, CrCr and VV, respectively, one important result is that the linkage of the Cp ligands causes an extra stabilization of the cationic species of **2b–d** as well as of **1b–d** compared to that of the parent compounds **2a** and **1a**. The heterobimetallic species **3** displays a cyclic voltammogram that resembles **1a** as well as **2a**. On the one side the cyclic voltammogram of **3** at ambient temperature contains a reduction step at $E°$ = −2047 mV, which is similar to $E°$(red.) of the homobinuclear V complex **1a**. On the other side an oxidation can be observed at $E°$ = −653 mV comparable to the first oxidation potential of the homobinuclear Cr complex **2a** (see Table I).

The reversibility of the oxidation step is shown by the peak current ratio of i_{pa}/i_{pc} = 1.00 (5). The difference of the peak potentials, ΔE_p = 60 mV, sustains a one-electron transfer like the first oxidation step of **2a**. In accordance to **3** its monocation **3PF$_6$** reveals the same cyclic voltammogram, which confirms the one-electron transfer involved in these redox pairs. In Figure 4 cyclic voltammograms of **3** are shown, which were recorded at ambient temperature. Unfortunately the redox couple of the reduction step contains a shoulder (marked with an asterisk) due to impurities, which became larger in the course of several measurements.[16]

In addition to these reversible redox pairs of **3** its cyclic voltammogram reveals a second oxidation wave, which is irreversible at ambient temperature (Figure 4B and Table I). The second oxidation at E_{pa} below +400 mV, which is in the region of the +1/+2 oxidation of VV and CrCr, is only partially reversible at low temperature. A comparison of the peak currents in Figure 4 points to a one-electron transfer for the irreversible oxidation step as well.

The mixed-metal compound VCr shows similar extended redox chemistry as the Cp-bridged VV complexes **1b–d** and the CrCr complex **2a** do and is stable within three different oxidation states on the cyclic voltammetric time scale encompassing 28–30 ve. The different oxidation states of the binuclear μ-Cot compounds **1–3**, which are completely reversible even at slow cyclic voltammetric scan rates (<50 mV/s), are summarized in Table II and include species containing 27–31 ve.

Oxidations of Cr-Containing Dinuclear μ-Cot Complexes. As well-known from the literature ferricinium cations can be used as convenient and powerful one-electron oxidation reagents in organometallic chemistry ($E°_{Cp_2Fe/Cp_2Fe^+}$ = +490 mV vs SCE in DME[17]). With respect to the redox potentials of the dinuclear μ-Cot complexes in this series containing Cr as a metal center, e.g. **2a** and **3**, it should be possible to prepare the corresponding monocations by the oxidation of the neutral complex with an appropriate amount of $(Cp_2Fe)PF_6$. In an equimolar reaction of the dinuclear μ-Cot derivatives **2a** as well as **3** with $(Cp_2Fe)PF_6$, it was possible indeed to synthesize the corresponding monocations (eq 3).

$$\underset{\substack{\textbf{2a: } M = M' = Cr \\ \textbf{3: } M = V,\ M' = Cr}}{(Cp_2MM')(\mu\text{-Cot})} + (Cp_2Fe)PF_6 \rightarrow \underset{\substack{\textbf{2aPF}_6 \\ \textbf{3PF}_6}}{[(Cp_2MM')(\mu\text{-Cot})]PF_6} + Cp_2Fe \quad (3)$$

In addition to the monooxidation, the cyclic voltammetric study of the Cp-bridged all-chromium complexes **2b–d** revealed an oxidation to a dication that was stable on the cyclic voltammetric time scale. In our first attempt to generate the dications we used $Ag(CF_3CO_2)$(AgTFA), anticipating to get a dication as a crystalline material. For example, we oxidized the $GeMe_2$-bridged derivative **2d** with AgTFA in acetone (eq 4). But the crystalline ma-

$$\textbf{2d} + 2AgTFA \rightarrow 2Ag + \textbf{2d(TFA)}_2 \quad (4)$$

terial of the dication was not stable enough to be isolated and handled at ambient temperature. Hence we decided to perform an in situ oxidation with an excess of $(Cp_2Fe)PF_6$ in an NMR tube at low temperature because small amounts of ferricinium cations should not impair the NMR measurements as much as a precipitate of elementary silver does (eq 5). The thermal stability of the di-

$$\textbf{2d} + 2(Cp_2Fe)PF_6 \xrightarrow[\text{acetone}]{T \le -80\ °C} \textbf{2d(PF}_6)_2 + 2Cp_2Fe \quad (5)$$

cation $\mathbf{2d}^{2+}$ is rather low, and the temperature-dependent ^{1}H NMR experiments show that it decomposes below −20 °C within a few minutes.

(15) Like **6** its permethylated derivative **7** is also subjected to a reversible one-electron oxidation, but its potential is shifted toward a more negative value: $E°(7/7^+)$ = −910 mV.[13a]

(16) In an additional experiment we studied the free ligand Cot cyclic voltammetrically and could observe an irreversible reduction peak at E_{pc} = −1940 mV vs SCE in DME at ambient temperature. Hence we assume the shoulder near the reversible reduction step of **3** in Figure 4B to be originated in the reduction of free Cot deliberated by the decomposition of **3** in the course of the cyclic voltammetric measurements.

(17) Elschenbroich, Ch.; Bilger, E.; Ernst, R. D.; Wilson, D. R.; Kralik, M. S. *Organometallics* **1985**, *4*, 2068.

Scheme I

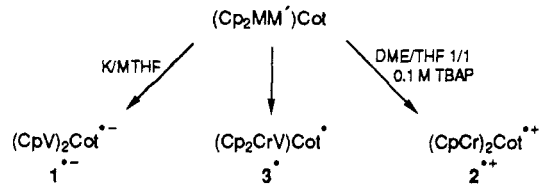

The dication $\mathbf{2d}^{2+}$ as well as the monocation $\mathbf{3}^{+}$, which are isoelectronic to the all-vanadium complexes VV, can be characterized by ^{1}H NMR spectroscopy while the monocation $\mathbf{2a}^{+}$ is paramagnetic and isoelectronic to **3** and therefore can be studied by ESR spectroscopy.

ESR Properties. Regarding the results of the cyclic voltammetric study, it should also be possible to generate the radical ions of **1** as well as of **2** with 29 and 31 ve. Indeed, upon contact of MTHF solutions of these compounds with a potassium mirror in a high vacuum sealed ESR tube, ESR-active radical anions were immediately formed (eq 6).

$$\underset{\mathbf{1, 2}}{\mathrm{MM}} \xrightarrow{K/MTHF} \underset{\mathbf{1^{\bullet-}, 2^{\bullet-}}}{\mathrm{MM^{\bullet-}}} \qquad (6)$$

For the dichromium anions $\mathbf{2a–d}^{\bullet-}$ the ESR activity still could be observed after several days, whereas for the divanadium anions $\mathbf{1a–d}^{\bullet-}$ the ESR signals could be measured after a year with nearly undiminished intensities, although these samples were allowed to stand at ambient temperature. The rapid generation of the radical anions upon contact with the potassium metal is in accordance to the relatively modest reduction potential obtained from the cyclic voltammetric study, and the stability of these radical anions confirms the reversibility of the electron transfer during the electrochemical reduction. On the other hand, the oxidation of the dichromium complex **2a** with $(FeCp_2)PF_6$ leads to the stable ESR-active monocation $[(CpCr)_2(\mu\text{-Cot})]^{\bullet+}$ containing 29 ve which could be isolated and proven by elemental analysis. The ESR properties of $\mathbf{2aPF_6}$ are exactly the same as those for $\mathbf{2a}^{\bullet+}$ generated in situ by reaction with 4-pyridinecarboxaldehyde or electrochemical oxidation. Therefore the in situ oxidation was also performed with the Cp-bridged dichromium compounds **2b–d** (eq 7). The stability of the

$$\underset{\mathbf{2a–d}}{\mathrm{CrCr}} \xrightarrow{\text{4-pyridinecarboxaldehyde}} \underset{\mathbf{2a–d^{\bullet+}}}{\mathrm{CrCr^{\bullet+}}} \qquad (7)$$

29 ve cations in solution, which still shows the same ESR activity after several days, again is in harmony with the electrochemical results. After all we are able to produce three different isoelectronic synfacial μ-Cot complexes bearing 29 ve (Scheme I). Unfortunately an electrochemical "in situ" oxidation of the divanadium complexes **1a–d** to 27 ve species in an ESR tube was unsuccessful although it was tried very carefully at low temperature. This failure may be due to the nearby second, but irreversible oxidation step observed in their cyclic voltammograms.

Liquid Solution Spectra of the 29 ve Species. The most striking feature of the radical anion spectra of the divanadium species $VV^{\bullet-}$ is their hyperfine structure (hfs) with 15 equidistant lines and the exceptional small hyperfine coupling constants (hfcc) $a(^{51}V) = 1.00 \pm 0.05$ mT (Table III). As an example of a typical radical spectrum of $VV^{\bullet-}$ the liquid solution spectrum of $\mathbf{1c}^{\bullet-}$ is shown in Figure 5A. The hfs is caused by the hf interaction of the unpaired electron with two equivalent V centers ($I(^{51}V) = {}^7/_2$), which implies a complete delocalization of the unpaired electron on both metal centers.

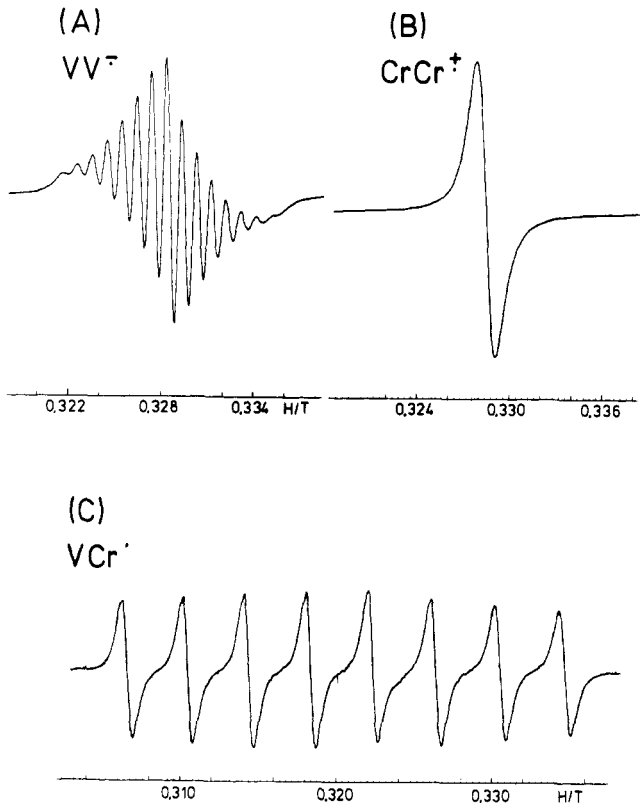

Figure 5. Fluid solution ESR spectra of $[X(Cp'_2MM')(\mu\text{-Cot})]^n$ containing 29 ve (X-band, T = 300 K): (A) n = 1−, X = $SiMe_2$, M = M′ = V ($\mathbf{1c}^{\bullet-}$), (MTHF); (B) n = 1+, X = $SiMe_2$, M = M′ = Cr ($\mathbf{2c}^{\bullet+}$) (acetone); (C) n = 0, X = H, H, M = V, M′ = Cr ($\mathbf{3}^{\bullet}$) (toluene) (notice that the gage of the three spectra is the same).

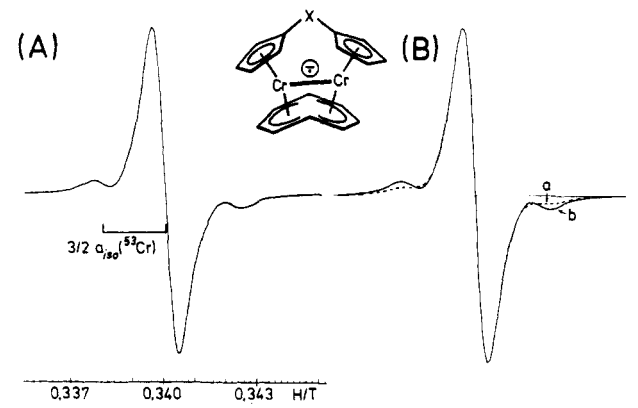

Figure 6. (A) Fluid solution ESR spectrum of $CrCr^{\bullet-}$ ($\mathbf{2c}^{\bullet-}$) obtained from K reduction in MTHF (T = 300 K, X-band). (B) Simulated spectra of $CrCr^{\bullet-}$ with 9.55% ^{53}Cr (---) and 19.1% ^{53}Cr (—). For more information consult text.

As can be seen from Figure 5B the fluid solution spectra of the isoelectronic dichromium monocations only consist of a single envelope. Unfortunately a ^{53}Cr hfs, which can be observed in numerous chromium sandwich compounds bearing one unpaired electron,[3b,18] cannot be detected in these cases because of the broad line width ($L_{p/p} \approx 1.3$ mT).

The feature of the fluid solution spectra of the neutral heterobinuclear 29 ve compound $VCr^{\bullet}$ ($\mathbf{3}^{\bullet}$) exists in an

(18) (a) Elschenbroich, Ch.; Gerson, F. *J. Organomet. Chem.* **1973**, *49*, 445. (b) Elschenbroich, Ch.; Gerson, F.; Stohler, F. *J. Am. Chem. Soc.* **1973**, *95*, 6956. (c) Elschenbroich, Ch.; Möckel, R.; Zenneck, U.; Clack, A. W. *Ber. Bunsenges. Phys. Chem.* **1979**, *83*, 1008. (d) Li, T. T.-T.; Kung, W.-J.; Ward, D. L.; McCullock, B.; Brubaker, C. H., Jr. *Organometallics* **1982**, *1*, 1229.

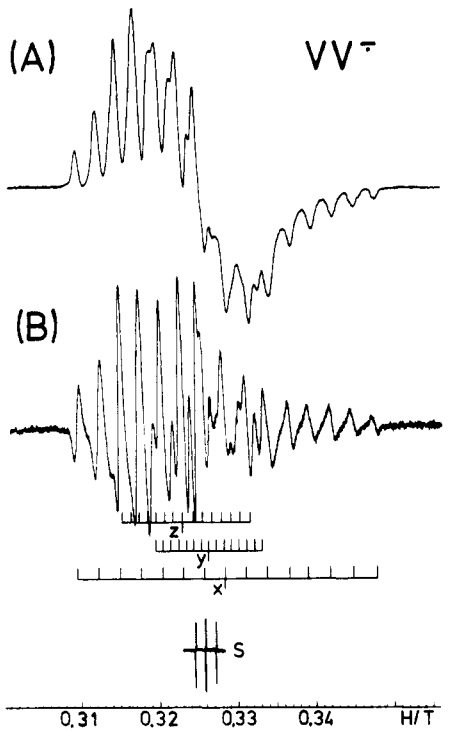

Figure 7. Frozen solution ESR spectra of $VV^{\bullet-}$ ($1c^{\bullet-}$) obtained from K reduction in MTHF: (A) first derivative spectrum; (B) second derivative spectrum (X-band) (T = 130 K, S = Fremy's salt).

8-line pattern due to the hfc of the unpaired electron with the vanadium nucleus (Figure 5C).

Liquid Solution Spectra of the 31 ve Species. A typical liquid solution spectrum of the K-reduced CrCr complexes **2a–d**$^{\bullet-}$ is shown in Figure 6A. It consists in a single line envelope symmetrically flanked by low- and high-field satellites originated from the hfc with ^{53}Cr. Due to the fairly broad line width it is difficult to distinguish between the localized or delocalized nature of the single electron. Therefore we computed a spectrum with a portion of 9.55% ^{53}Cr representing the localization of the unpaired electron on one Cr-center as well as a spectrum with a portion of 19.1% ^{53}Cr showing the delocalized case.[19] From Figure 6B it is obvious the theoretical spectrum with 19.1% ^{53}Cr fits the experimental spectrum in Figure 6A proving the delocalized nature of the unpaired electron in $CrCr^{\bullet-}$, which is also in line with the small isotropic ^{53}Cr hfcc ($a(^{53}Cr)$ = 1.38 + 0.01 mT).[20]

Frozen Solution Spectra. On cooling the ESR samples, frozen solution spectra could be obtained in all cases (Figures 7–9). The special feature of the frozen solution spectra of $VV^{\bullet-}$ (Figure 7) is a multitude of lines effected by the hfc with two vanadium nuclei. For the inner resonance line overlap, the second derivative spectrum is depicted additionally (Figure 7B). One g component (g_x)[21] in the frozen solution spectra of VV^- shows a fairly large

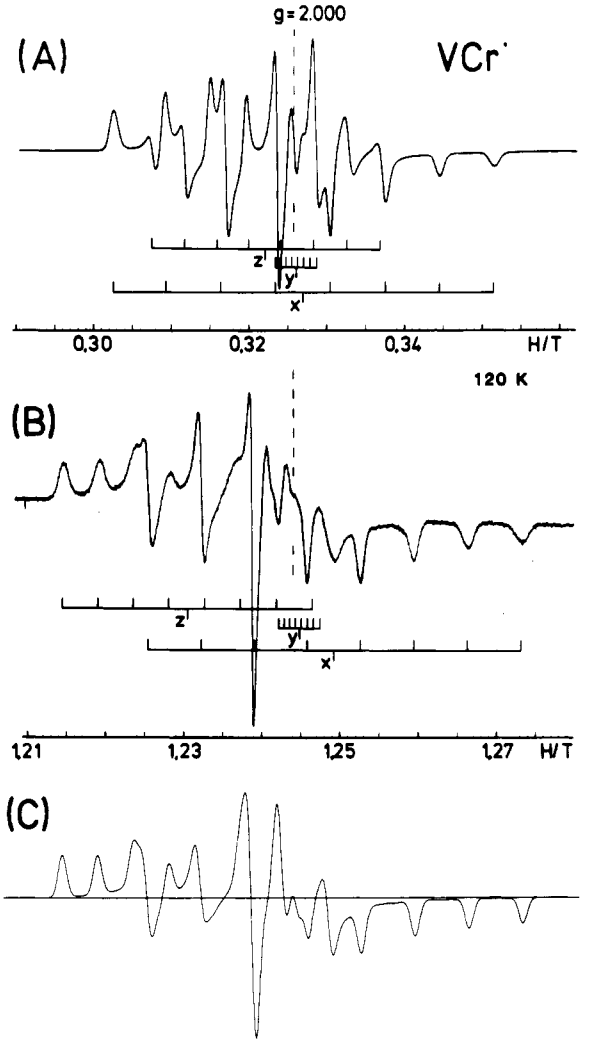

Figure 8. Frozen solution ESR spectra of VCr (3$^{\bullet}$) (toluene, T = 130 K): (A) X-band spectrum; (B) Q-band spectrum; (C) simulated spectrum of (B).

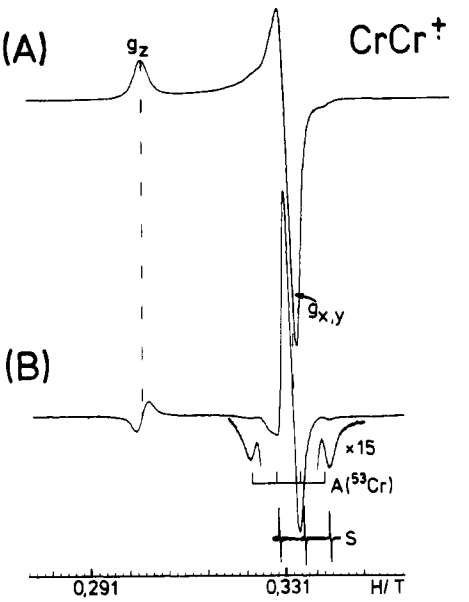

Figure 9. Frozen solution ESR spectra of $CrCr^{\bullet+}$ ($2c^{\bullet+}$) (X-band) (acetone, T = 130 K): (A) first derivative spectrum; (B) second derivative spectrum (S = Fremy's salt).

^{51}V hfcc, and its 15-line pattern can be observed unchanged down to $T \geq 10$ K, confirming the complete delocalization of the unpaired electron even at very low temperatures,

(19) The probability of the electron coupling with one ^{53}Cr center will double if the single electron is delocalized on both of the metal centers.

(20) In sandwich-like mononuclear chromium radicals isotropic ^{53}Cr hfcc can be found with $a(^{53}Cr)$ = 1.7–2.0 mT (see ref 3b, 18).

(21) Although for a rhombic system the principal directions of the magnetic tensors with respect to the molecular structure cannot be determined from the frozen solution spectra directly, we define the principal components of the **g** tensor in accordance to the mononuclear bent vanadocenes with respect to the following definition of the system of coordinates: the z direction is represented by the metal–metal bonding vector and the x axis is directed normal to the molecular mirror plane containing the two metal centers (vide infra, see also ref 22, 23).

(22) Petersen, J. L.; Dahl, L. F. *J. Am. Chem. Soc.* **1975**, *97*, 6416.

(23) Petersen, J. L.; Griffith, L. *Inorg. Chem.* **1980**, *19*, 1852.

Table II. Observed Reversible Redox States of the Dinuclear μ-Cot Complexes 1–3, Arranged by the Number of Valence Electrons (ve)

	31 ve		30 ve		29 ve		28 ve		27 ve
2a–d	$CrCr^-$	$\overset{-e^-}{\rightleftharpoons}$	CrCr	$\overset{-e^-}{\rightleftharpoons}$	$CrCr^+$	$\overset{-e^{-a}}{\rightleftharpoons}$	$CrCr^{2+}$		
3			VCr^-	$\overset{e^-}{\rightleftharpoons}$	VCr	$\overset{-e^-}{\rightleftharpoons}$	VCr^+		
1a–1d					VV^-	$\overset{-e^-}{\rightleftharpoons}$	VV	$\overset{-e^{-b}}{\rightleftharpoons}$	VV^+

[a] Irreversible for **2a** at ambient temperature and reversible at −27 °C. [b] Irreversible for **1a**; reversible for **1b–d** at −37 °C.

Table III. ESR Data[a] for the Binuclear μ-Cot Radical Complexes $[X(Cp'_2MM')\text{-}(\mu\text{-}Cot)]^n$

compounds			g values[b,c]					metal hyperfine coupling constants, mT			
			g_{iso} ($10^3\Delta g_{iso}$)	g_x ($10^3\Delta g_x$)	g_y ($10^3\Delta g_y$)	g_z ($10^3\Delta g_z$)	⟨g⟩	a_{iso}	A_x	A_y	A_z
n = 1−	M = M′ = V	X = H,H (**1a**⁻)	2.0059 (5) (3.6)	1.989 (2) (−13)	2.006 (2)[d] (4)	2.022 (2)[d] (20)		^{51}V 1.049 (5)	(∓)2.85 (3)	(±)0.84[e]	(∓)1.17 (5)[d]
		X = CH_2 (**1b**⁻)	2.0058 (5) (3.5)	1.988 (2) (−14)	2.007 (2)[d] (5)	2.023 (2)[d] (21)		1.040 (5)	(∓)2.99 (3)	(±)1.12[e]	(∓)1.25 (5)[d]
		X = $SiMe_2$ (**1c**⁻)	2.0061 (5) (3.8)	1.9898 (5) (−12.5)	2.0019 (5)[f] (−0.4)	2.0266 (5)[f] (24.3)	2.0059	0.950 (5)	(∓)2.73 (3)	(±)0.86 (3)[f]	(∓)1.18 (3)[f]
		X = $GeMe_2$ (**1d**⁻)	2.0065 (5) (4.3)	1.990 (2) (−12)	2.005 (2)[d] (3)	2.024 (2)[d] (22)		1.006 (5)	(∓)2.76 (3)	(±)0.80[e]	(∓)1.22 (5)[d]
n = 1+	M = M′ = Cr	X = H,H (**2a**⁺)	2.0240 (5) (21.7)	2.009 (1) (7)		2.057 (1) (55)	2.025	^{53}Cr no.	1.20 (5)		no.
		X = CH_2 (**2b**⁺)	2.0237 (5) (21.4)	2.009 (1) (7)		2.056 (1) (54)	2.024	no.	1.25 (5)		no.
		X = $SiMe_2$ (**2c**⁺)	2.0244 (5) (22.1)	2.009 (1) (7)		2.057 (1) (55)	2.025	no.	1.19 (5)		no.
		X = $GeMe_2$ (**2d**)⁺	2.0243 (5) (22.0)	2.010 (1) (8)		2.057 (1) (55)	2.026	no.	1.19 (5)		no.
n = 0	M = Cr, M′ = V	X = H,H (**3**)	2.0039 (5) (1.6) 2.0036 (5)[g] (1.3)	1.9906 (2)[g] (−11.7)	2.0004 (5)[f] (−1.9)	2.0215 (2)[g] (19.2)	2.0042	^{51}V 4.03 (1)	6.91 (5)[g]	0.73 (5)[f]	4.60 (5)[g]
n = 1−	M = M′ = Cr	X = H,H (**2a**⁻)	1.9545 (5) (−478)	1.977 (1) (−25)		1.911 (1) (−91)	1.955	^{53}Cr 1.38 (1)	2.37 (5)	0.66[e]	1.11 (10)
		X = CH_2 (**2b**⁻)	1.9573 (5) (−45.0)	1.980 (1) (−22)		1.912 (1) (−90)	1.957	1.39 (1)	2.40 (5)	0.66[e]	1.10 (10)
		X = $SiMe_2$ (**2c**⁻)	1.9545 (5) (−47.8)	1.978 (1) (−24)		1.909 (1) (−93)	1.955	1.37 (1)	2.35 (5)	0.67[e]	1.09 (10)
		X = $GeMe_2$ (**2d**⁻)	1.9550 (5) (−47.3)	1.978 (1) (−24)		1.909 (1) (93)	1.955	1.39 (1)	2.45 (5)	0.60[e]	1.12 (10)
				1.9797 (5)[g]	1.9765 (5)[g]	1.9091 (5)[g]	1.955				

[a] Obtained from X-band spectra unless otherwise mentioned. [b] The hfcc and g values were determined from liquid solution spectra at T = 298 K, whereas from the frozen solution spectra at T = 130 ± 5 K; the g values were determined with respect to second-order effects. [c] $\Delta g_i = g_i - g_e$, where i = iso, x, y, or z and g_e = 2.0023. [d] Calculated from the experimental spectra according to the best fit of the spectrum of **1c**. [e] Calculated from $A_y = 3 \times a_{iso} - A_x - A_z$. [f] Obtained from the best fit. [g] Taken from Q-band spectra; no. = not observed.

which let us assume a mixed-valence class III for the $VV^{\bullet-}$ anions.[24] The low resolution of the inner part of these spectra makes it impossible to appoint the other g and ^{51}V hf components exactly despite the second derivative spectra.

Therefore we tried to estimate the remaining g as well as A values from computer-simulated spectra. But although a great deal (several hundreds) were computed, e.g. for $\mathbf{1c}^{\bullet-}$, only a moderate conformity to the experimental spectra could be achieved finally. The impossibility to get fairly good agreement between the computed and the experimental spectra is probably predominantly caused by two effects: (i) we have to expect an anisotropic ^1H hfs with two different sets of Cp protons and three different sets of Cot protons, if the Cot ring is fixed in rigid solution, which are not resolved but would effect the line widths of various g components differently, and (ii) due to the low symmetry, C_{2v} or C_s, of the binuclear radicals it may happen also that the principle values of the **g** as well as ^{51}V hf tensors are not exactly coaxial.[22] But nevertheless from the computed spectra it is safe to assume a rhombic **g** and ^{51}V hf tensor, and with a degree of certainty g_z and the corresponding A_z could be determined, whereas g_y and $A_y(^{51}V)$ were taken from the "best" fit of the calculated spectra. The averaged g value, $\langle g \rangle = {}^1/_3\,(g_x + g_y + g_y)$, agrees well with g_{iso} for $\mathbf{2c}^{\bullet-}$ (see Table 3).

Three g values are also obtained from the frozen solution spectra of the heterobinuclear metal complex $VCr^{\bullet}$ (Figure 8). Whereas from the X-band spectrum (Figure 8A), it is difficult to determine the g and $A(^{51}V)$ values, g_x and g_z as well as the corresponding ^{51}V hfcc can be gathered from the Q-band spectra directly (Figure 8B; Table III), and the remaining g_y and $A_y(^{51}V)$ values were obtained from a calculated spectrum (Figure 8C). Similar to $VV^{\bullet-}$ the agreement between the calculated and the experimental spectra is only passably good, owing to the reasons mentioned above. Again the particular g_i values of VCr are very similar to the corresponding g_i values of $VV^{\bullet-}$, corroborating the distinct localization of the unpaired electron on the V center in VCr. In harmony with the results of $VV^{\bullet-}$ too, the high-field g component ($g_x = 1.9906$) shows the largest ^{51}V hfcc $A_x = 6.91$ (5) mT and the low-field component $g_z = 2.0215$ has a somewhat smaller ^{51}V hfcc $A_z = 4.60$ (5) mT. g_y is almost equal to the spin-free value and shows only a poor ^{51}V hf interaction ($A_y = 0.73$ (5) mT).

The X-band frozen solution spectra of the isoelectronic 29 ve $CrCr^{\bullet+}$ radical cations $\mathbf{2a-d}^{\bullet+}$ surprisingly only consists of two g values despite the low molecular symmetry (Figure 9). This feature still remained if the spectra were recorded on a Q-band spectrometer. As the symmetry of the **g** tensor is determined by the surrounding electrical charge distribution, the two g values in the ESR spectra of $CrCr^{\bullet+}$ reflect an axial or almost axial electron distribution around the metal–metal bond, pointing out that the intermetal bond can be influenced only to a small extent by the low symmetric ligand field in $CrCr^{\bullet+}$.

Compared to the vanadium radicals $VV^{\bullet-}$ as well as $VCr^{\bullet}$ the low-field g component is shifted even more downfield ($g_z = 2.057$) whereas the high-field component is close to g_e ($g_{x,y} = 2.009$) (Table III). A ^{53}Cr hfs is only observable on $g_{x,y}$, which can be made clearer in a second derivative spectrum (Figure 9B). Because of the broad line width, the ^{53}Cr hfcc can solely be estimated to $A_{x,y}(^{53}Cr) = 1.20$ (5) mT, which is rather small compared to $A_\perp(^{53}Cr)$ of mononuclear Cr sandwich radicals.[18] Hence, the small

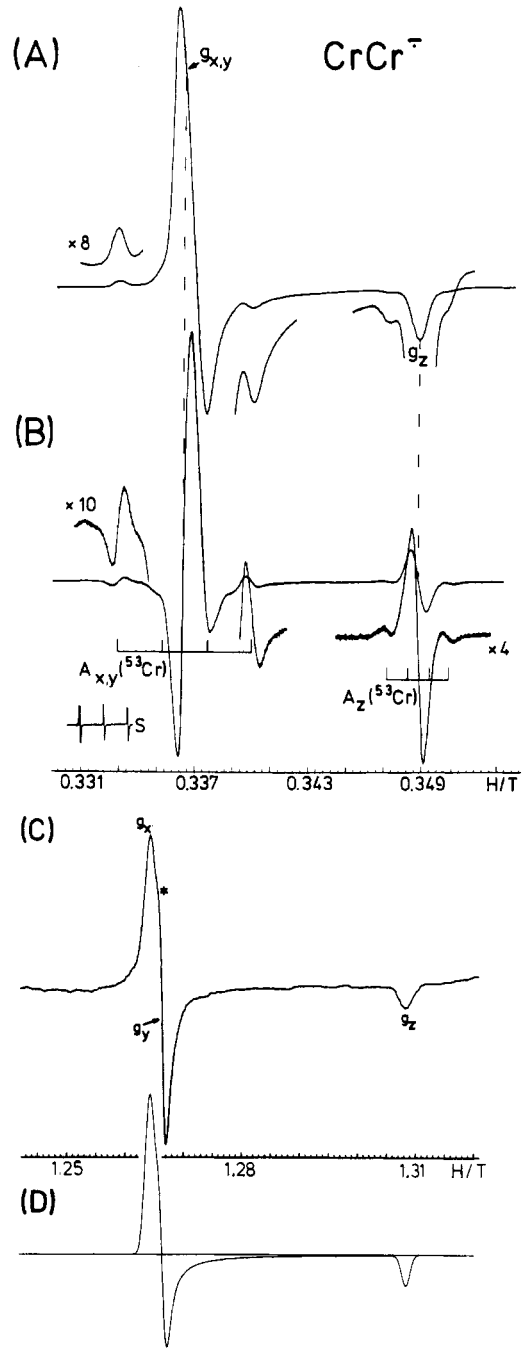

Figure 10. Frozen solution ESR spectra of $CrCr^{\bullet-}$ ($\mathbf{2d}^{\bullet-}$) obtained from K reduction in MTHF (T = 130 K): (A) X-band spectrum, first derivative; (B) X-band spectrum, second derivative; (C) Q-band spectrum (note the appearance of a shoulder in the strong absorption line marked with an asterisk; it proves two g values for $g_{x,y}$, which are not exactly equal); (D) computer simulation of the Q-band spectrum (S = Fremy's salt).

$A_{x,y}(^{53}Cr)$ values of $CrCr^{\bullet+}$ indicate a delocalization of the unpaired electron on both Cr centers. The relative intensities of the main signal and its ^{53}Cr satellites at $g_{x,y}$ suggest that two different g values coincide accidentally: one with and the other without an observable Cr hfs (compare the relation of the resonance line of $CrCr^{\bullet-}$ in Figure 10, vide infra).

Just the inverse spectra were obtained for the 31 ve $CrCr^{\bullet-}$ anions $\mathbf{2a-d}^{\bullet-}$. Again from the X-band spectra an axial **g** tensor seems to appear with one strongly upfield shifted g_z value ($g_z = 1.910 \pm 2$) and one g component near to g_e ($g_{x,y} = 1.978 \pm 2$) (Figure 10A). But the Q-band spectra of $CrCr^{\bullet-}$ shows an additional shoulder on the

(24) Robin, M. B.; Day, P. *Adv. Inorg. Chem. Radiochem.* **1967**, *10*, 247.

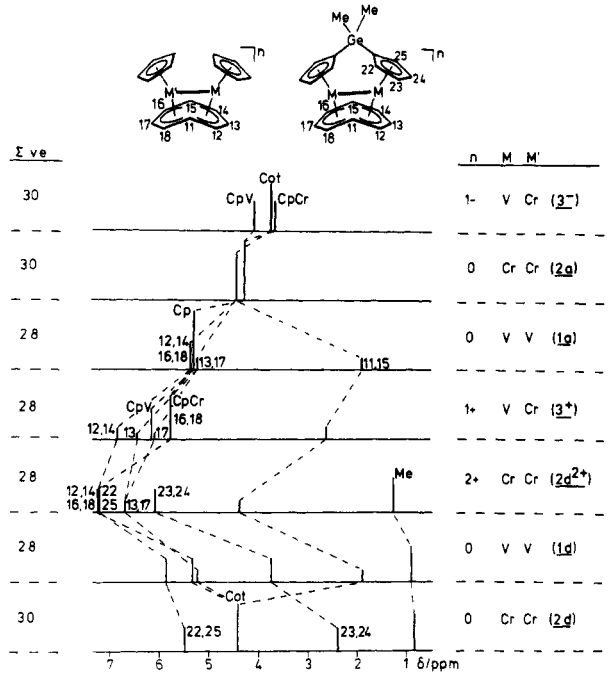

Figure 11. ^{1}H NMR stick diagram of some complexes of [X-(CP'$_2$MM'(μ-Cot)]^n.

strong resonance line of $g_{x,y}$, indicating two different g values which are attested by a computer simulation of the Q-band spectrum (Figure 10C,D; Table III). The perturbation of the axial symmetrical charge distribution of the metal–metal bond in CrCr$^{\bullet-}$ by the ligand field, although larger than in CrCr$^{\bullet+}$, still remains very small.

$g_{x,y}$ as well as g_z show weak satellites originated from ^{53}Cr hfc, and because of the relative intensities, it must be accepted that the resolved ^{53}Cr hfs on $g_{x,y}$ only belongs to one g component. Unfortunately, the growing line width upon increasing the magnetic field prevents a resolution of the ^{53}Cr hfs in the Q-band spectra, making a univocal assignment of the large ^{53}Cr hfcc in Figure 10A impossible. The relative intensities of the main resonance line of g_z and its ^{53}Cr satellites again point to a complete delocalization of the single electron in CrCr$^{\bullet-}$ in a rigid state as well (compare the relative intensities in the liquid solution spectrum in Figure 6).

NMR Properties. All of the even-numbered charged and uncharged μ-Cot complexes in this series are diamagnetic at low temperature, allowing us to obtain ^{1}H as well as ^{13}C NMR spectra. Illustrating the shift range of the binuclear μ-Cot compounds **1–3**$^-$ with 28 and 30 ve, a stick diagram of some proton NMR spectra recorded at T = 200 K is shown in Figure 11, and the corresponding ^{1}H and ^{13}C NMR data are listed in Table IV.

Regarding the number of resonance lines, the ^{1}H NMR spectra of the Cp bridged derivatives **1b–d** and **2b–d** agree with an averaged molecular C_{2v} symmetry of these complexes in solution, whereas the molecular structure in the solid state obeys C_1 or C_s symmetry at best. In the crystalline structure the bridging group X is strongly tilted toward one of the bridging Cot carbons. Hence, the protons of the substituents R and R' of the bridging group X as well as the two proximal and distal protons H(22,25) and H(23,24), respectively, are in magnetically distinct regions.[4,5] But from the NMR spectra a molecular fluxionality is indicated, in which the bridging group X = ERR' is wagging from one side to the other, equilibrating the axial and equatorial positions of X as well as the different proximal and distal Cp protons (Scheme II). In most cases

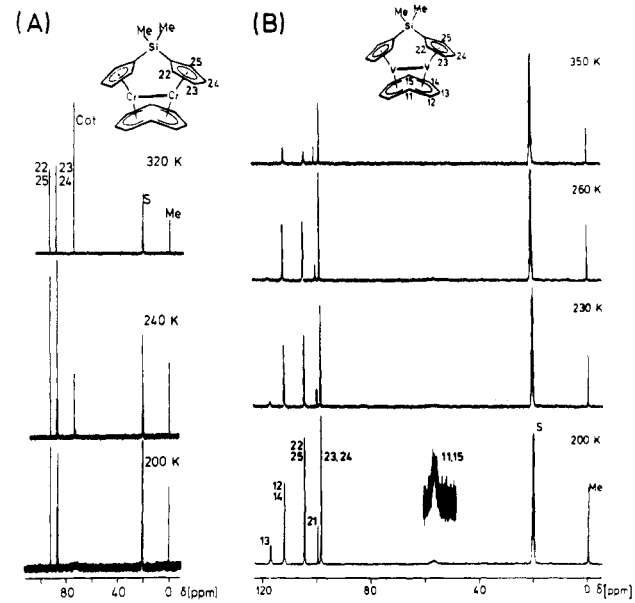

Figure 12. Temperature-dependent ^{13}C NMR spectra of $Me_2Si(Cp'M)_2$ (μ-Cot): (A) M = Cr (**2c**); (B) M = V (**1c**) (400 MHz, [$^2H_8$]toluene ≙ S).

Scheme II

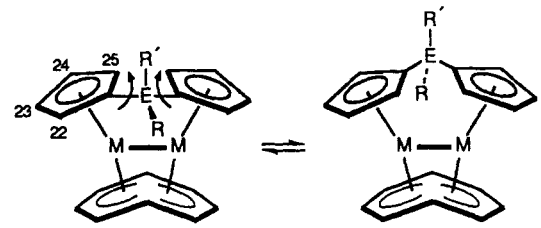

the resonance signals can be directly assigned to the related Cot and Cp protons by means of their integrals.

The different Cp protons of the X-bridged derivatives were assigned by NOE experiments because the averaged distance of the protons of X is definitely smaller to the proximal protons H(22,25) than to the distal protons H(23,24); e.g., in the case of **2b** the averaged distance H(X)–H(22,25) is about 280 pm whereas H(X)–H(23,24) = 490 pm, and H(X)–H(22,25) = 320 pm and H(X)–H(23,24) = 550 pm for **2c**.[5] The extra high-field shifted absorption at δ < 2 ppm for VV is assigned to H(11,15) of the bridging Cot position since from the molecular structure it can be shown that the bonding vectors of C(11)–H(11) and C(15)–H(15) decline from the planes C(8–12) and C(14–16), respectively, by a considerable amount, whereas the bonding vectors of the other CH groups are almost in plane with the three adjacent Cot carbon atoms.[2–5] Hence, for the bridging carbons C(11,15) a more extensive change from an sp^2 to an sp^3 hybridization has to come about compared to the other carbons of the Cot ligand. This suggestion is confirmed by the low-temperature ^{13}C NMR spectra of the VV compounds: one broad absorption at δ = 57 ppm is clearly high-field shifted by about 60 ppm from the typical range of the residual Cot signals at δ > 110 ppm (Figure 12) which were assigned by ^{1}H,^{13}C-selective decoupling experiments. Unfortunately the line width of the high-field-shifted signal is too broad to get resolved $^1J_{C-H}$ spin–spin coupling constants providing clear-cut information about the change of hybridization compared to the other $^1J_{C-H}$ coupling constants of the Cot ligand. The ^{13}C resonance lines of the Cp ligands in the X-bridged compounds were also assigned by ^{1}H,^{13}C-selective decoupling experiments.

Table IV. NMR Data for the Binuclear μ-Cot Complexes $[X(Cp'_2MM')(\mu\text{-Cot})]^{n}$ [a]

compounds			^{1}H NMR shifts[d]					
			Cp		Cot			
			H(22,25)	H(23,24)	H(11,15)	H(12,14,16,18)	H(13,17)	others
$n = 0$	M = M′ = V	X = H,H (**1a**)	4.97 (10 H)		1.79 (2 H)	5.2 (2 H)	4.90 (2 H) t	...
			5.31 (10 H)[b]		1.90 (2 H)	5.31 (2 H)	5.23 (2 H) t	...
			5.30 (10 H)[c]		1.89 (2 H)	5.33 (2 H)	5.22 (2 H) t	...
		X = CH_2 (**1b**)	5.27 (4 H)	3.21 (4 H)	1.80 (2 H)	5.27 (6 H)		5.20 (2 H)
		X = $SiMe_2$ (**1c**)	5.43 (4 H)	3.45 (4 H)	1.70 (2 H)	5.23 (4 H)	4.99 (2 H) t	0.92 (6 H)
								0.86 (6 H)
		X = $GeMe_2$ (**1d**)	5.51 (4 H)	3.44 (4 H)	1.80 (2 H)	5.26 (4 H)	4.97 (2 H) t	0.92 (6 H)
			5.86 (4 H)[b]	3.75 (4 H)	1.90 (2 H)	5.34 (4 H)	5.23 (2 H) t	0.86 (6 H)
$n = 2+$	M = M′ = Cr	X = $GeMe_2$ (**2d**$^{2+}$)	7.21 (4 H)[b]	6.09 (4 H)	4.40 (2 H)	7.25 (4 H)	6.70 (2 H)	1.27 (6 H)
$n = 1+$	M = V, M′ = Cr	X = H,H (**3**$^+$)	6.13 (5 H)		2.61 (2 H)	6.84 (2 H)	6.41 (1 H)	
			5.75 (5 H)			5.75 (2 H)	6.07 (1 H)	
$n = 0$	M = M′ = Cr	X = H,H (**2a**)	3.90 (10 H)			4.23 (8 H)		...
			4.29 (10 H)[b]			4.45 (8 H)		...
			4.27 (10 H)[c]			4.43 (8 H)		...
		X = CH_2 (**2b**)	5.00 (4 H) t	1.59 (4 H) t		4.42 (8 H)		4.42 (2 H)
		X = $SiMe_2$ (**2c**)	4.94 (4 H) t	1.98 (4 H) t		4.22 (8 H)		0.72 (6 H)
		X = $GeMe_2$ (**2d**)	5.00 (4 H) t	1.88 (4 H) t		4.21 (8 H)		0.80 (6 H)
			5.49 (4 H) t[b]	2.4 (4 H) t		4.42 (8 H)		0.83 (6 H)
$n = 1-$	M = V, M′ = Cr	X = H,H (**3**$^-$)	4.10 (5 H)			3.76 (8 H)		
			3.68 (5 H)					

compounds			^{13}C NMR shifts δ ($^1J_{^{13}C-^1H}$, Hz)							
			Cp			Cot			^{51}V NMR[e]	
			C(22,25)	C(23,24)	C(21)	C(11,15)	C(12, 14,16,18)	C(13,17)	others	δ	$\delta\nu_{1/2}$, KHz
$n = 0$	M = M′ = V	X = H,H (**1a**)		98.2		no.	112.4	117.1			
		X = CH_2 (**1b**)	100.03	92.67	109.28	57.2	110.05	118.50	33.5 (CH_2)	+1245 (200 K)	1.2
			(175)	(175)			(160)	(160)	(143)		
		X = $SiMe_2$ (**1c**)	104.71	98.71	99.95	57.2	112.08	117.11	−0.24 ($SiMe_2$)	+1283 (200 K)	1.5
										+1140 (298 K)	13.8
		X = $GeMe_2$ (**1d**)	103.97	98.23	102.37	56.8	112.37	117.05	1.36 ($GeMe_2$)	+1295 (200 K)	1.8
										+1080 (298 K)	26.3
$n = 0$	M = M′ = Cr	X = H,H (**2a**)		86.62			74.59				
				(173)			(157)				
		X = CH_2 (**2b**)	88.88	83.40	96.94		74.29		32.18 (CH_2)		
		X = $SiMe_2$ (**2c**)	92.57	87.27	87.55		73.86		−0.46 ($SiMe_2$)		
			(173)	(172)			(162)		(121)		
		X = $GeMe_2$ (**2d**)	92.27	86.07	90.65		74.06		1.28 ($GeMe_2$)		

[a] If not noted otherwise, the complexes were dissolved in $[^2H_8]$toluene and measured at $T = 200$ K; the shifts were referenced to δ(Ph-C*H*D_2) = 2.03 ppm relative to TMS for ^{1}H NMR and δ(Ph-$^{13}CD_3$) = 20.4 ppm relative to TMS for ^{13}C NMR. [b] In $[^2H_6]$acetone, to δ($CH_3C(O)CD_3$) = 2.04 relative to TMS. [c] In $[^2H_8]$THF, referenced to δ($CD_2CHDCD_2CD_2O$) = 1.73 ppm relative to TMS. [d] Resolved ^{1}H,^{1}H spin–spin coupling only could be observed in some cases, and then they are signed with the splitting mode, e.g. t for triplet. [e] Relative to $VOCl_3$; from ref 25.

Additionally ^{51}V NMR shifts[25] of **1b–d** are listed in Table V and show an exceptional low-field shift δ(200 K) >+1200 ppm, which is very unusual for organovanadium complexes in low oxidation states.[26]

Discussion

Cyclic Voltammetry. The cyclic voltammetric results on the synfacial complexes VV and VCr as well as CrCr are in certain contrast to the findings of the antifacial compounds $[(CpM)_2(\mu\text{-Cot})]^n$ (M = Ru, n = 0; M = Co, Rh, n = 2+) wherein the oxidation step occurs in a two-electron transfer involving a structural metamorphosis.[11a,27] This structural rearrangement, which mostly is accompanied by a larger cyclic voltammetric peak separation,[11a,28] allows a more extensive metal–metal interaction to be essential as the number of valence electrons has been decreased by oxidation. Concerning the ΔE_p values of the synfacial compounds, which normally range from 58 to 81 mV irrespective of the scan rate ($20 \le v \le 200$ mV) (see Table I), we assume no significant structural rearrangement during the electrochemical reactions. Moreover, a structural rearrangement is not necessarily required because in the synfacial configuration the metal centers already are in the most proper position for a metal–metal interaction. Hence, their molecular structures should resemble the structures confirmed by the single-crystal X-ray structure determinations.[2–5] Furthermore it is noteworthy that Cp-bridged CrCr compounds show four different stable oxidation states in cyclic voltammetric measurements even at ambient temperature including 31 to 28 ve. From the literature only very few examples of dinuclear organometallics are known featuring such a pronounced redox chemistry, i.e. $[(CpM)(\mu\text{-NO})]_2^n$ (M = Co, Rh; n = 2+, 1+, 0, 1−)[29] and the dithiolene complex $(Cp^*Ni)_2(\mu\text{-}C_2S_4)$.[30]

More than four cyclic voltammetric stable oxidation states in dinuclear organometallic complexes could only be observed for dicobalt triple-decker sandwiches[31,32] and fulvalene-bridged diiron dibenzene complexes.[33] Such an extended flexibility of the oxidation states in dinuclear organometallic compounds seems to be a special characteristic of sandwich-like complexes.[34] But all of these dinuclear species possess "electron rich" metals like Fe, Co, Rh, and Ni, whereas the Cp-bridged Cot complexes **2b–d** to our knowledge are the first examples of organometallic dinuclear compounds that present four electrochemically stable oxidation states with the "electron-poor" transition-metal chromium. As mentioned previously strong metal–metal interactions, e.g. metal–metal multiple bonds as well as doubly bridging ligands, are the most important factors supporting the stability of di- and polynuclear compounds in very different oxidation states:[35] the bridging ligands keep the metal centers together like a pair of tongs while the metal–metal multiple bonds are able to distribute the charge over both the metal centers which results in a reduced effective charge on each metal center. These requirements are fulfilled for chromium complexes **2b–d**, and additionally the chromium centers are coordinated with polyene ligands, which are also able to stabilize metal centers in different oxidation states.[34]

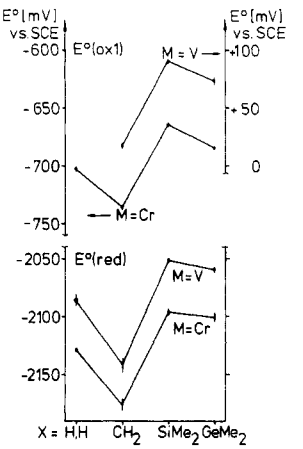

Figure 13. Correlation between the redox potentials $E°$ and the Cp-bridging function X in $X(Cp'_2M_2)(\mu\text{-Cot})$ (M = V, Cr **1a–2d**). X = H,H represents the case without direct linkage between the Cp ligands. The length of the lines shows the standard deviation.

The assumption of an extensive delocalization of charge in the case of the dichromium ions is consistent with the two distinctly spaced one-electron waves for the oxidation steps 0/+1 and +1/+2 ($\Delta E°$ > 1000 mV, see Table I).[36] Approximately large differences between two successive oxidation or reduction steps were observed in $\{[V(CO)_4](\mu\text{-}EMe_2)\}_2$ (E = P, As) ($\Delta E°$ = 600–700 mV)[37] and $[(CpCo)(\mu\text{-NO})]_2$ ($\Delta E°$ = 830 mV),[29] wherein metal–metal double bonds must be considered with respect to the 18 ve rule for each metal center.

Unlike the Cp-bridged CrCr complexes **2b–d** the corresponding VV species **1b–d** only reveal cyclic voltammograms exhibiting one reversible and close to it a second irreversible oxidation at low temperature. This marked difference is in accordance to the assumption that—with respect to the VV complexes—in the CrCr analogoues the additional two electrons fill an antibonding MO reducing the metal–metal bond order of 3 in **1a** to an order of 2 in **2a** as mentioned briefly in the Introduction (see also below). Therefore in the two one-electron oxidations in **2a** and its related complexes two electrons are removed stepwise from an antibonding MO whereas in **1a** and its Cp-bridged derivatives two electrons are removed stepwise from a bonding MO. This results in an enhancement of the bond order in the dichromium species but in a decrease in the divanadium species, which at last leads to a relative destabilization of the cationic VV species compared with that of the corresponding CrCr cations. This conception is in line with the relative values of the first oxidation

(25) Rehder, D., private communication.
(26) (a) Kidd, R. G. In *Annu. Rep. NMR Spectrosc.* **1978**, *10a*, 2 and references cited therein. (b) Rehder, D.; Wieghart, K. *Z. Naturforsch., B* **1981**, *36B*, 1251.
(27) Edwin, J.; Geiger, W. E.; Salzer, A.; Ruppli, U.; Rheingold, A. L. *J. Am. Chem. Soc.* **1987**, *109*, 7893.
(28) Heinze, J. *Angew. Chem.* **1984**, *96*, 823. Geiger, W. E. *Prog. Inorg. Chem.* **1985**, *33*, 275.
(29) Connelly, N. G.; Payne, J. D.; Geiger, W. E. *J. Chem. Soc., Dalton Trans.* **1983**, 295.
(30) Maj, J. J.; Rae, A. D.; Dahl, L. F. *J. Am. Chem. Soc.* **1982**, *104*, 4278.
(31) Brennan, D. E.; Geiger, W. E. *J. Am. Chem. Soc.* **1979**, *101*, 3399.
(32) Edwin, J.; Bochmann, M.; Böhm, M. C.; Brennan, D. E.; Geiger, W. E.; Krüger, C.; Pebler, J.; Pritzkow, H.; Siebert, W.; Swiridoff, W.; Wadepohl, H.; Weiss, J.; Zenneck, U. *J. Am. Chem. Soc.* **1983**, *105*, 2582.
(33) Astruc, D. *Acc. Chem. Res.* **1986**, *19*, 377 and literature cited therein.
(34) Geiger, W. E.; Connelly, N. G. *Adv. Organomet. Chem.* **1984**, *23*, 1; **1985**, *24*, 87.
(35) Vahrenkamp, H. *Angew. Chem.* **1975**, *87*, 363; **1978**, *90*, 403.
(36) (a) From the literature it is known that in dinuclear complexes two well-separated one-electron waves ($\Delta E°$ > 500 mV) can be observed, which occur in a stepwise reduction or oxidation due to strong metal–metal interactions (e.g. metal–metal multiple bonds). Upon decreasing interactions, the potential difference $\Delta E°$ between the two waves decreases and finally results in a single two-electron wave (compare ref 31 and literature cited therein and ref 36b). (b) Order, N. V., Jr.; Geiger, W. E.; Bitterwolf, T. E.; Rheingold, A. L. *J. Am. Chem. Soc.* **1987**, *109*, 5680.
(37) Madach, T.; Vahrenkamp, H. *Chem. Ber.* **1981**, *114*, 505; and **1981**, *114*, 513.

Table V. Selected Bond Lengths[a] of X(Cp'M)$_2$(μ-Cot) Complexes Obtained by X-ray Structure Determination

	d_{M-M}	d_{C-E}[b]	$d_{M-C(21-25)}$	$d_{M-C(12,14,16,18)}$	$d_{M-C(13,17)}$	$d_{M-C(11,15)}$	ref
M = V							
X = H,H (**1a**)	243.9 (1)		226.9 (15)	212.8 (6)	219.9 (6)	224.6 (6)	2a
X = $SiMe_2$ (**1c**)	243.0 (1)	185.6 (3)	229.1 (10)	213.5 (9)	220.6 (6)	225.4 (6)	5
		185.4 (3)					
M = Cr							
X = H,H (**2a**)	239.0 (2)		219 (2)	206 (1)	210 (1)	226 (1)	3a
X = CH_2 (**2b**)	234.3 (1)	150.4 (4)	221 (2)	208 (1)	212.7 (4)	225.6 (4)	5
		150.8 (3)					
X = $SiMe_2$ (**2c**)	238.3 (2)	186.0 (7)	221 (2)	208 (1)	213 (1)	227 (1)	5

[a] In pm. [b] Bond length between the carbon C(1) of the Cp ligand and the bridging atom E of the bridging function X (E = C, Si).

potential: the CrCr complexes are easier to oxidize by about 730–750 mV than the corresponding isostructural VV complexes.

From a more detailed inspection of the $E°$ values of the different reversible redox couples, it can be ascertained that the $E°$ values generally become more positive in the series CH_2 < H,H < $GeMe_2$ < $SiMe_2$ as the bridging function X wherein H,H represents the cases of the parent compounds **1a** and **2a** without any direct linkage between the Cp ligands (Figure 13, Table I). An exception can be observed for $E°$ (ox.$_2$) of the chromium species. Whereas $E°$ (ox.$_2$) of the Cp-bridged complexes was established at ambient temperature and still accomplishes this ordering, $E°$ (ox.$_2$) of compound **2a** was obtained at low temperature and therefore it is not comparable to the other $E°$(ox.$_2$) values directly. An identical sequence of $E°$ values was reported for the oxidation of X-bridged (η^6-benzene)tricarbonylchromium complexes in the literature previously.[38]

From spectroscopic and theoretical studies it is well-known that in contrast to alkyl groups Si and Ge groups behave as π-acceptors wherein the Si substituents are stronger π-acceptors than the corresponding Ge substituents.[39] The observed dependence of $E°$ values from the electron-withdrawing ability of the bridging group X points to a small but remarkable admixture of the Cp ligand orbital to the HOMO and LUMO[40-42] which is in line with MS Xα results of Weber et al.[43] The electronic effect of the bridging group X can also be stated from the ^{51}V hyperfine coupling constants of **1a–d**$^{\bullet-}$ which increase within 10% in the series **1c**$^{\bullet-}$ < **1d**$^{\bullet-}$ < **1a**$^{\bullet-}$ < **1b**$^{\bullet-}$ (Table III) as well as from the ^{13}C NMR shifts of the resonance signals of C(22,25) and C(23,24) (Table IV). The different influence of X on the ^{13}C NMR shifts can be explained by the π interaction of the filled π bonds of the aromatic system and the low-lying empty d orbitals of the bridging atoms Si and Ge or the σ^* MO of the Si,C bond and the Ge,C bond.[44]

Another noteworthy characteristic of the redox behavior of VV and CrCr can be established by comparing the differences ($\Delta E°_1$) between the two redox couples, $E°$ (red.) and $E°$ (ox.$_1$). $\Delta E°_1$ increases to a small but noticeable extent in the sequence $GeMe_2$ > (H,H) > $SiMe_2$ > CH_2

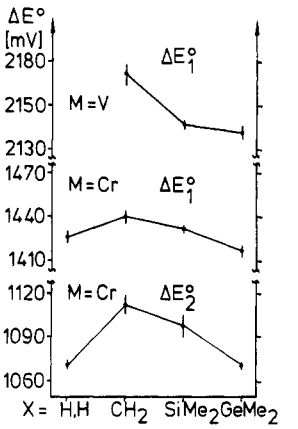

Figure 14. Correlation between the differences ($\Delta E°$) of two consecutive redox pairs and the Cp-bridging function X in X-(Cp'$_2$M$_2$)(μ-Cot) (M = V, Cr; **1a–2d**). X = H,H represents the case without direct linkage between the Cp ligands (for details see text).

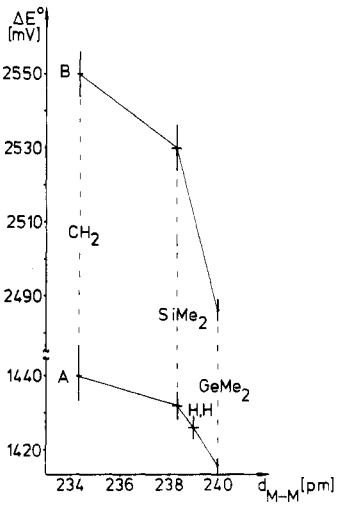

Figure 15. Correlation between the difference of the reduction and the first oxidation potential (A) as well as the reduction and second oxidation potential (B) and the metal–metal distance (d_{M-M}) in X(Cp'$_2$Cr$_2$)(μ-Cot) complexes: X = H,H (**2a**), CH_2 (**2b**), $SiMe_2$ (**2c**), $GeMe_2$ (**2d**). For **2d** the intermetal distance d_{M-M} = 240 pm was estimated (see ref 45). The length of the lines represents the standard deviation.

(H,H is put into parentheses because only for the Cr species two consecutive reversible redox couples are found) (see Table I and Figure 14). An identical sequence in $\Delta E°$ can be observed between $E°$ (ox.$_1$) and $E°$ (ox.$_2$) for CrCr (see $\Delta E°_2$, Figure 14), which is more pronounced. This ordering of the $\Delta E°$ data as a function of the bridging group X obviously does not agree with its electronic properties as it was obtained for $E°$ values of the redox couples. But rather there exists a correlation between $\Delta E°$ and the metal–metal bond length d_{M-M}.

(38) Rieke, R. D.; Tucker, I.; Milligan, S. N.; Wright, D. R.; Willeford, B. R.; Radonovich, L. J.; Eyring, M. W. *Organometallics* **1982**, *1*, 938.
(39) (a) Sipe, H. J., Jr.; West, R. *J. Organomet. Chem.* **1974**, *70*, 367. (b) Bock, H.; Alt, H. *Chem. Ber.* **1970**, *103*, 1784.
(40) (a) Clack, W. D.; Warren, K. D. *Struct. Bonding (Berlin)* **1980**, *39*, 1. (b) Hebendanz, N.; Köhler, F. H.; Müller, G.; Riede, J. *J. Am. Chem. Soc.* **1986**, *108*, 3281.
(41) (a) Heilbronner, E.; Bock, H. *Das HMO-Modell und seine Anwendung*; Verlag Chemie: Weinheim, 1968. (b) Triechel, P. M.; Mueh, H. J.; Bursten, B. E. *Isr. J. Chem.* **1977**, *15*, 253.
(42) (a) Bedard, R. L.; Dahl, L. F. *J. Am. Chem. Soc.* **1986**, *108*, 5933. (b) Colbran, S. B.; Robinson, B. H.; Simpson, J. *Organometallics* **1984**, *3*, 1344.
(43) Weber, J.; Chermette, H.; Heck, J. *Organometallics*, following paper in this issue.
(44) Bullpitt, M.; Kitching, W.; Adcock, W.; Doddrell, D. *J. Organomet. Chem.* **1976**, *116*, 161.

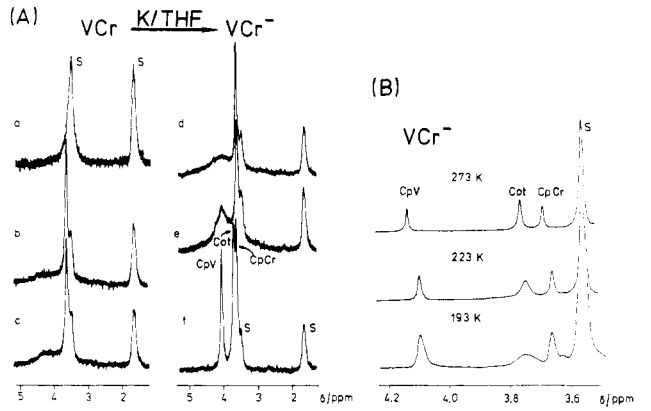

Figure 16. (A) ^1H NMR spectra of stepwise reduced VCr (**3**•) with potassium in [$^2H_8$]THF (S) (T = 300 K, 60 MHz). (B) Expanded ^1H NMR spectra of **3**$^-$ in [$^2H_8$]THF at various temperatures showing the Cot ring rotation decelerated at very low temperature (400 MHz).

From X-ray structure determinations on some of these complexes[2-5] it is shown that an increase of the bond length in the bridging function causes a small elongation of the intermetal bond length (see Table V). As between the chromium complexes **2c** and **2a**, a similar small elongation of the metal–metal distance between the vanadium species **1c** and **1a** can be observed (see Table V), and hence there are good reasons to assume a change in the metal–metal bond length (d_{M-M}) for VV resembling that for the corresponding CrCr complexes. A correlation between the $\Delta E°_1$ values and d_{M-M} is shown in Figure 15A for CrCr. A more pronounced effect will be noted if the difference of the reduction potential and the second oxidation potential is taken into account (Figure 15B).

Since the potentials of the oxidation and reduction steps in electrochemical studies are closely related to the energy of the HOMO and LUMO,[41,46] the potential difference ($\Delta E°_1$) represents a measure of the HOMO - LUMO splitting, which especially may hold for very similar complexes. Therefore the correlation between $\Delta E°_1$ and d_{M-M} found in Figure 15 obviously points to an increasing HOMO - LUMO splitting with decreasing intermetal bond length, which is in good agreement to the MS Xα results.[43]

ESR. From ESR spectroscopic results some references can be made about the metal–metal interaction in these closely related dinuclear radical complexes VV$^-$, VCr, and CrCr$^+$. The most important difference between the homobinuclear radical anions VV$^{•-}$ (**1a–d**$^{•-}$) and the heterobinuclear complex VCr• (**3**•) is revealed by the ^{51}V hfcc: $a(^{51}V)$ of VCr• is about four times larger than $a(^{51}V)$ of VV$^{•-}$ (Table III).[47] Such a strong increase in $a(^{51}V)$ on

Chart II

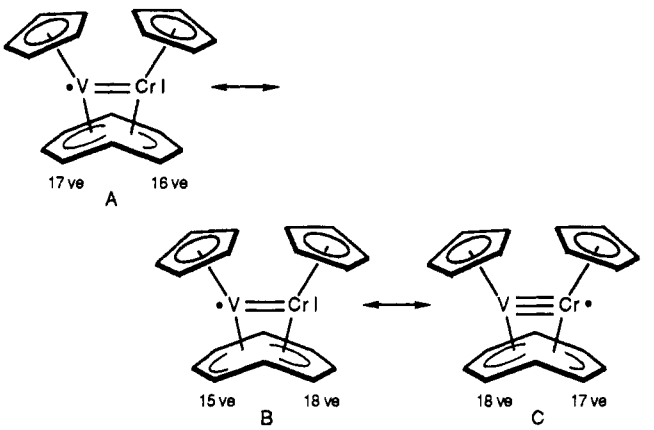

going from VV$^{•-}$ to VCr• points to an essential localization of the unpaired electron on the vanadium center in the heterobinuclear complex **3**•. This is also confirmed by a comparison of the corresponding isotropic g values g_{iso}: g_{iso}(VCr•) is almost equal to those of all vanadium radical anions VV$^{•-}$ but different from g_{iso} of the CrCr$^{•+}$ cations markedly (Table III).

Another plain argument for the essential localization of the unpaired electron on one metal center could be obtained from an ^1H NMR experiment. In radicals without conjugated π bondings the proton hfcc strongly depend on the distance of the protons to the paramagnetic center resulting in different shifts and line widths of the corresponding signals in the ^1H NMR spectra.[50] Hence upon successive reduction of the paramagnetic complex VCr• (**3**•) to its diamagnetic anion VCr$^-$ (eq 8), a varied narrowing

$$\underset{\substack{\mathbf{3}^{•}\\ \text{paramagnetic}}}{[(Cp_2VCr)(\mu\text{-Cot})]^{•}} \xrightarrow{K/[^2H_8]\text{-THF}} \underset{\substack{\mathbf{3}^{-}\\ \text{diamagnetic}}}{[(Cp_2VCr)(\mu\text{-Cot})]^{-}} \quad (8)$$

of the proton resonance signals of the different Cp groups should be observed if the unpaired electron will be mainly localized on one metal center and the electron exchange between **3**$^-$ and **3**• is fast compared to that on the NMR time scale. In Figure 16A the ^1H NMR spectra of **3**• upon successive reductions with potassium in [$^2H_8$]THF are depicted certifying the considerations mentioned above: the resonance line of one Cp group sharpens earlier than the other and earlier than that of the Cot ligand. The assignment of the Cp as well as of the Cot resonance signals can be made definitely by their intregrals in the 400-MHz spectrum (Figure 16B). The single line of the Cot ligand indicates its fast rotation, which equilibrates the proton positions. Compared to the NMR time scale this rotation causes an intermediate coordination of each of the Cot carbon atoms to the paramagnetic V center resulting in a direct spin delocalization on each of the Cot protons as it occurs for the Cp ligand linked to the paramagnetic center. Therefore the paramagnetic line broadening of the Cot protons is comparable to that of the Cp protons.

Following the resonance structures of VV and CrCr (Vide supra) from the V-centered single electron two resonance structures of VCr• are possible (Chart II). In addition a third resonance structure (C) shows the un-

(45) Regarding the small metal–metal bond lengthening upon increasing the bond distance in the Cp-bridging group on going from **2b** to **2c**, the Cr–Cr bond length in the $GeMe_2$-bridged derivative can be estimated to ~240 pm if the Ge–C bond length is assumed to be 198 (3) pm.

(46) Bard, A. J. *Pure Appl. Chem.* **1971**, *25*, 379.

(47) The extremely small ^{51}V hfcc in VV$^{•-}$ may be explained mainly by a distinct increase of the 4S contribution to the SOMO as also mentioned by Weber and co-workers.[43] An increase of 1% in the 4s contribution should change $a(^{51}V)$ by almost +1 mT.[48] This strong effect of the 4s contribution was also evidenced by Evans and co-workers for Cp_2VX_2, wherein the 4s character of the unpaired electron increases from 1.3% in Cp_2VCl_2 to 1.9% in Cp_2VEt_2 changing the $a(^{51}V)$ values from −7.35 mT to −6.24 mT.[49] Therefore the blatant difference in the ^{51}V hfcc of VV$^{•-}$ and VCr is explained not only by the delocalization and localization of the unpaired electron but also by the negative charge in VV$^{•-}$ compared to that in VCr•, which will enhance the 4s character of the unpaired electron. In accordance to these considerations the sign of isotropic ^{51}V hfcc for VCr• like for other bent vanadocenes[23,49] should be negative whereas for VV$^{•-}$ negative or positive.

(48) Goodman, B. A.; Raynor, J. B. *Adv. Inorg. Chem. Radiochem.* **1970**, *13*, 135.

(49) Evans, A. G.; Evans, J. C.; Espley, D. J. C.; Morgan, P. H.; Mortimer, J. *J. Chem. Soc., Dalton Trans.* **1978**, 57.

(50) La Mar, G. N. In *NMR of Paramagnetic Molecules, Principles and Applications*; La Mar, G. N., Horrocks, W. D., Jr., Holm, R. H., Eds.; Academic Press: New York, 1973; p 85 ff. Horrocks, W. Dew., Jr., *Ibid.* p 127 ff.

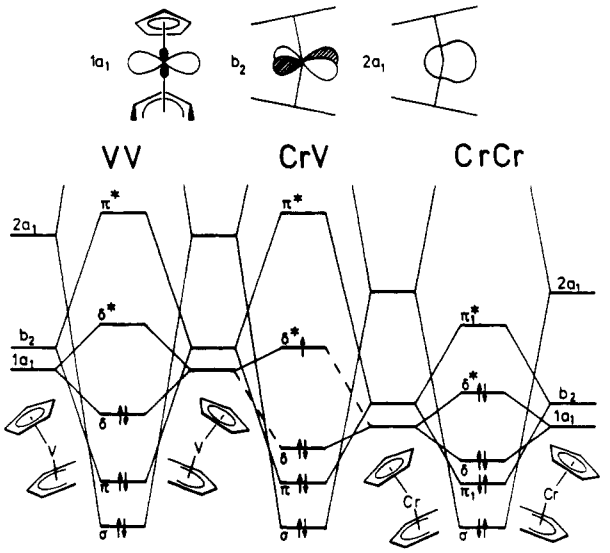

Figure 17. Qualitative interaction diagram of the frontier orbitals of two (η^5-Cp)M(η^5-C_5H_5) units (M = V, Cr) borrowed from the MO diagram of bent metallocenes (see ref 51).

paired electron on the Cr center making allowance for certain spin density on Cr. Because of the larger ve difference in B, and especially considering a stronger bonding interaction between the vanadium atoms and the bridging carbon atoms C(11) and C(15) in VV compared to the corresponding CrC bond in CrCr (Table V, vide infra), the bonding relations in VCr• are best described by A.

Due to the distinct g anisotropy of the frozen solution spectra, metal-centered radicals are to be assumed for the 29 ve as well as for the 31 ve species and the averaged g values, $\langle g \rangle = {}^1/_3(g_x + g_y + g_z)$, are in passably good agreement with g_{iso} obtained from the liquid solution spectra (Table III). The latter suggests no remarkable structural change between the liquid and the frozen solution state, which is in harmony with the delocalized nature of the unpaired electron in the liquid as well as in the rigid solution. Since the liquid solution ESR spectra of VV•⁻, VCr•, and CrCr•⁺ show fairly narrow line widths at ambient temperature and their g_{iso} values are near the spin-free value, orbitally nondegenerate ground states are indicated for these μ-Cot radical complexes. This is not surprising with respect to the C_{2v} symmetry for the homobinuclear and C_s symmetry for the heterobinuclear complexes and can be accommodated by a simplified model of the metal–metal interaction. The μ-Cot complexes **1–3** can be built up by two semiopen metallocenes wherein the metal centers share two bridging carbon atoms of the μ-Cot ligand.

Regarding the deviation of 10–20° from the parallel disposition of the Cp ligand and the related η^5-Cot unit, the individual electron configuration of a $CpMC_5H_5$ unit may be deduced from the bent metallocenes wherein the degeneracy of the e_{2g} orbital of pure metallocenes is removed. On the basis of Lauher's and Hoffmann's MO description for bent metallocenes[51] the interaction diagram of the frontier orbitals, which are responsible for the metal–metal bonding characteristics, is depicted qualitatively in Figure 17. The $2a_1$ MO's of the individual metal fragments are predestinated for a strong metal–metal σ bond, whereas the overlap of the two b_2 orbitals leads to a π-type MO. A small bonding interaction can be assumed from the combination of the two $1a_1$ orbitals which results in a metal–metal δ-type MO. In accord to the η^5:η^5 bonding mode of the Cot ligand in **1a** and the bonding description of metallocenes, 22 ve are needed to fill up the ligand–metal MO. In the case of VV the remaining 6 ve fill the three metal bonding orbitals. Hence, a formal VV triple bond can be attributed to the configuration $\sigma^2\pi^2\delta^2$. This qualitative picture of the V,V bond in **1** agrees well with the results of MS Xα calculations performed by Weber et al.[43,52] If the metal centers are chromium, the additional two electrons will fill the δ* MO, reducing the formal metal–metal bond order to a double bond.

On forming the ESR active 29 ve species the δ* MO is only singly occupied (SOMO) and its nondegenerate nature is in accord with the ESR properties of these radicals. In line with this MO picture the principle localization of the unpaired electron on the V center in **3**• can be accommodated as well. Since the $1a_1$, b_2, and $2a_1$ orbitals for bent chromocenes are lower in energy than the corresponding V orbitals, the interaction of the $1a_1$ orbitals forming the δ bond will become worse and the "bonding" δ-type MO will mainly be of Cr nature whereas the δ*-type MO, which is singly occupied in VCr, mainly retains the nature of the V center. This situation is consistent with the two resonance structures A and B of VCr (vide supra).

Some hints at the relative proximity of the energy levels of the frontier orbitals can be obtained from the g values of the frozen solution spectra. In case of an unpaired electron in a nondegenerate orbital of pure metal character the deviation of the three g values from g_e can be expressed as shown in eq 9[48,53] or for the isotropic g value as shown in eq 10. From the sign of Δg_i it can be deduced whether

$$g_i = g_e + \Delta g_i = g_e + n_i/\Delta E_i \qquad (9)$$

$$i = x, y, z$$

$$g_{iso} = g_e + {}^1/_3\Sigma_i \Delta g_i = g_e + {}^1/_3\Sigma_i\, n_i/\Delta E_i \qquad (10)$$

the contributions of excited states arise from an interaction of the unpaired electron with filled MO ($E_o > E_n$) resulting in $g_i > g_e$ or with empty orbitals ($E_o < E_n$) resulting in $g_i < g_e$.

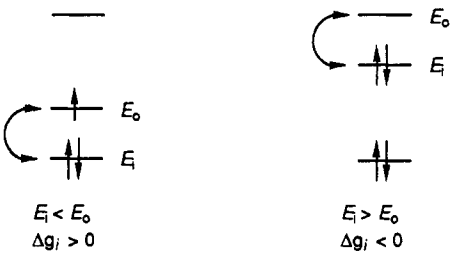

Taking into account that the oxidation state of each metal center of the μ-Cot complexes increases by 1 on going from VV•⁻ to CrCr•⁺, ξ_{Cr}(CrCr•⁺) would nearly be twice as large as ξ_V(VV•⁻) where ξ_v(VCr•) lies in between.[54] With

(51) Lauher, J. W.; Hoffmann, R. *J. Am. Chem. Soc.* **1976**, *98*, 1729.

(52) In the meantime two ab initio MO calculations were published for **1a** (see: Lüthi, H. P.; Bauschlicher, Ch. W., Jr. *J. Am. Chem. Soc.* **1987**, *109*, 2046. Mougenot, P.; Demuynck, J.; Benard, M.; Bauschlicher, Ch. W., Jr. *J. Am. Chem. Soc.* **1988**, *110*, 4503), but their results are inconsistent with experimental findings and fundamental calculations on the V_2 molecule. For some critical remarks see ref 43.

(53) n_i is a numerical factor whose magnitude depends on which orbitals may mix with the singly occupied MO (SOMO), and ξ_k is the spin–orbit coupling factor of the metals, which allows the ground state to mix with the excited states. ΔE_i is the energy separation between the SOMO (E_o) and the orbitals E_n, which may mix by spin–orbit coupling ($\Delta E_i = E_o - E_i$).

(54) The spin–orbit coupling factors ξ_k for the metal ions are $\xi_V(V^{2+}) \approx 170$ cm^{-1} and $\xi_V(V^+) = 136$ cm^{-1} and $\xi_{Cr}(Cr^{2+}) = 230$ cm^{-1} and $\xi_{Cr}(Cr^{3+}) = 273$ cm^{-1} (see ref 48). Presuming (i) a formal oxidation state of 2 for each metal center in the neutral complexes **1–3** and (ii) the reduction of the oxidation state in VV•⁻ to 1.5 and an increase to 2.5 in CrCr•⁺ for each center, the spin–orbit coupling factors ξ_V can be estimated to be $\xi_V(VV^{\bullet-}) \approx 150$ cm^{-1} and $\xi_{Cr}(CrCr^{\bullet+}) \approx 250$ cm^{-1}.

regard to the relative values of ξ_k and eq 9 from the g_x values, a growth in ΔE_x must be considered in the order $VCr^{\bullet} \approx VV^{\bullet-} < CrCr^{\bullet+}$ whereas the increase in g_z shows a decrease of the energy gap ΔE_z between the SOMO and the filled MO in the order $VCr^{\bullet} \gtrsim VV^{\bullet-} > CrCr^{\bullet+}$ if we assume the same numerical factor n_i for the corresponding g_i. From the increasing interaction of the SOMO δ^* with the filled MO on one side and the decreasing interaction with the higher lying empty MO on the other side upon enhancing the positive charge, a larger diminution of the δ,δ^* splitting compared to the σ,σ^* and π,π^* splitting of the metal–metal bond on going from $VV^{\bullet-}$ to $CrCr^{\bullet+}$ must be considered.

While the interaction of the half-filled orbitals in the 29 ve complexes obviously mainly occurs with lower lying filled MO, which after all can be seen also by the isotropic values ($g_{iso} > g_e$), just the opposite comes true for the 31 ve anions $CrCr^{\bullet-}$, wherein the single electron is filled in the π^*-type orbital (Figure 17). The high-field shift of $g_{x,y}$ is due to predominant interactions of the SOMO with the empty MO.

In virtue of these results it generally can be suggested that the frontier orbitals of the synfacial μ-Cot complexes are in relatively close proximity up to δ^* but are distinctly spaced from higher empty orbitals, i.e. π^* or σ^*, which is in harmony with the results of the MX Xα calculation.[43] This characteristic will be of great importance for the magnetic behavior of the species with even numbers of valence electrons (vide infra).

NMR. One remarkable feature developed by the stick diagram in Figure 11 is the different behavior of the Cot ligands. We note that for the 30 ve species CrCr as well as VCr^- the coordinated Cot only shows one singlet, which corresponds to the single Cot resonance line in the ^{13}C NMR spectra, indicating its fast rotation. Such a fluxionality of a Cot ligand could also be found in all kinds of synfacial "electron-rich" binuclear μ-Cot complexes containing 34 ve.[55] On the contrary the 28 ve species VV as well as VCr^+ have different Cot absorptions of the relative intensities 2:1:1 and 2:1:1:2:2, respectively, which is in harmony to the $\eta^5{:}\eta^5$-bonding mode of the Cot ligand shown by the molecular structure,[2-5] and demonstrates the rigidity of the Cot ring in the 28 ve complexes. The fixed nature of the cyclopolyolefin ligand can still be observed at $T = 330$ K for VCr^+ while the growing line width of the spectra of VV upon increasing temperatures allows the anisochrony of the Cot signals to be observed only up to $T = 280$ K. Nevertheless, from the ^{13}C NMR spectra the rigidity of Cot on VV can be followed till $T = 350$ K (Figure 12).

In the case of the CrCr derivatives a freezing of the Cot rotation is intimated by the line broadening of its resonance signal below $T = 240$ K in Figure 18B, but different Cot absorptions cannot be recognized before the temperature is cooled below $T = 160$ K.[4,5] A fixed Cot ligand in binuclear μ-Cot complexes at $T > 200$ K, in which all of the Cot carbons are linked to metal centers, hitherto could be regarded solely for antifacial derivatives.[27,55]

The rigidity of the Cot ligand in the synfacial 28 ve complexes at relative high temperature stands for its stronger connection with the metal centers compared to the 30 ve species. This also is proved by the molecular structure of **1** and **2**: the metal–carbon bond lengths normally enlarge distinctly on going from VV to CrCr, but on the contrary the interatomic distances between the metal centers and the bridging carbons C(11,15) are almost

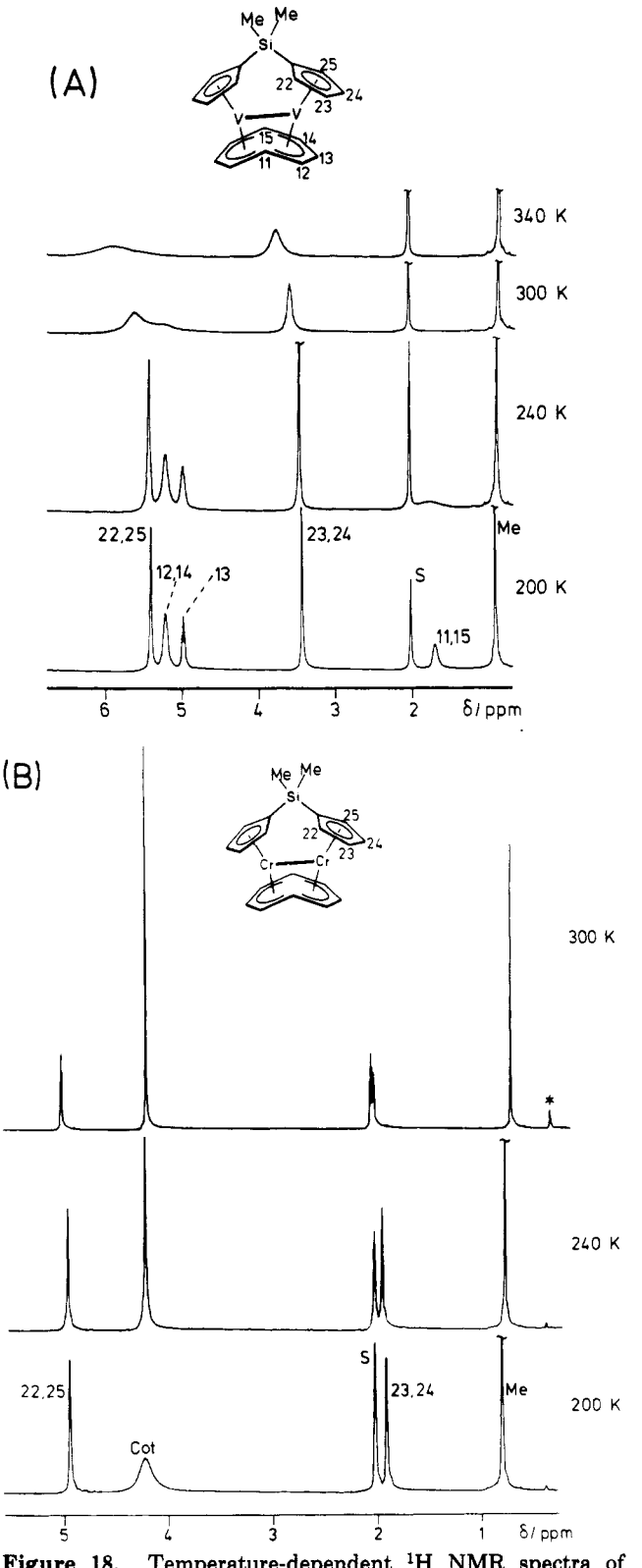

Figure 18. Temperature-dependent ^1H NMR spectra of $Me_2Si(Cp'M)_2(\mu\text{-Cot})$: (A) M = V (**1c**); (B) M = Cr (**2c**) (400 MHz, $[^2H_8]$toluene $\hat{=}$ S, the asterick = grease).

equal or for VV even somewhat shorter (Table V). This tighter linkage of Cot is to be attributed to a stronger Lewis acidity of the "electron poorer" metal centers in VV compared to those in CrCr.

Another ^1H NMR characteristic of the synfacial μ-Cot complexes can be borrowed from the charge dependency of the shifts. From Figure 11 we can generally state a low-field shift with increasing positive charge, which best can be followed for H(11,15) of the 28 ve complexes. The

(55) (a) Bieri, J. H.; Egolf, T.; von Philipsborn, W.; Piantini, U.; Prewo, R.; Ruppli, U.; Salzer, A. *Organometallics* **1986**, *5*, 2413.

Chart III

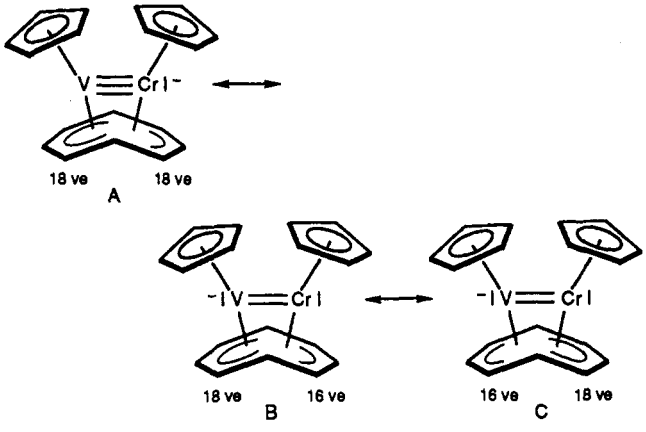

Chart IV

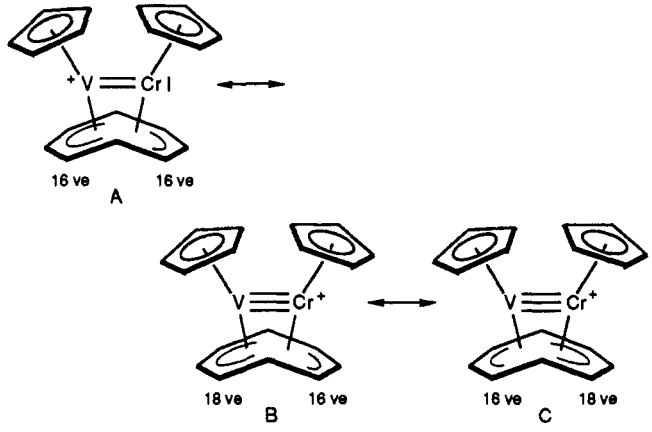

charge-induced shifts of the various Cot protons turn out differently (Table IV), but for the entire Cot ligand on the average a low-field shift of 1 ppm per unit charge can be estimated, which is comparable to the charge–shift correlation found for mononuclear sandwich compounds.[56] A similar effect is observed for the Cp protons of $\mathbf{2d}^{2+}$ compared to **1d**: the resonance line of the distal protons H-(23,24) of the dication is low-field shifted by about 2.34 ppm compared to that of the corresponding VV derivative. The effect of the charge on the proximal protons (22,25) is distinctly smaller (1.35 ppm), and hence the averaged low-field shift is 1.85 and 0.93 ppm per unit charge.

The shift difference between a neutral and a dicationic species enlarges even more if we compare **2d** and $\mathbf{2d}^{2+}$: the absorption line of the proximal protons of the dication is shifted low field by about 1.72 ppm from the corresponding line of the neutral derivative whereas the shifts of the distal protons even vary by about 3.69 ppm. This unusual low-field shift obviously is caused by two effects: (i) the charge-induced shift and (ii) the valence electron (ve) induced shift evoked by different valence electron numbers. The electron density on the metal centers is smaller by two electrons in VV compared to that in CrCr. Thus, the extent of the electron releasing from the metal centers onto the ligands must be less in the 28 ve species resulting in a deshielding of the Cp protons relative to the corresponding protons of the 30 ve complexes. The effect best can be seen by comparing the Cp resonances of **2a** and **1a**: on lowering the ve number from 30 to 28 a low-field shift of the Cp protons of about 1 ppm occurs. In contrast the average shifts of the Cot lines almost seem to be unaffected, which may be due to the different bonding characteristics of the Cot ligand in VV and CrCr (vide supra).

The valence-electron- and charge-induced shifts may help us to understand the various chemical shifts in VCr^+ as well as VCr^- and to make some attempts on charge distributions in these complex ions. Because of the fact that the paramagnetic center in VCr is allocated to the vanadium from the successive reduction to VCr^-, the ^1H NMR absorption of the CpV group can be assigned clearly to 4.1 ppm. Hence, the high-field shift of the CpV resonance amounts 1.2 ppm relative to VV (**1a**) while for CpCr the high-field shift amounts only to 0.61 ppm relative to CrCr (**2a**). For estimating the charge-induced shift, it must be taken into account that the shift of the CpV absorption of the 30 ve species VCr^- is referenced to the 28 ve complex **1a** on the one hand and the shift of the CpCr signal is referenced to the isoelectronic complex **2a** on the other hand. Remembering the valence-electron-induced high-field shift of 1 ppm on going from a 28 to a 30 ve species, the charge-induced shift of CpV in VCr^- is only about 0.2 ppm whereas it remains 0.61 ppm for CpCr, suggesting the negative charge is located on the Cr center predominantly. This charge distribution is best described by the resonance structure A, wherein both of the metal centers have 18 ve (Chart III). A distinct localization of the negative charge on the Cr center correlates also with the second metal ionization potentials of V and Cr.[57] The resonance structures B and C make contributions to a certain negative charge on the V center.

If we look at the Cp resonance signals of the 28 ve species VCr^+, we note that they are shifted to a low field with respect to the neutral homobinuclear compounds **1a** and **2a**. With the assumption of the same net effect on the shifts of each of the CpM groups changing from VCr^- to VCr^+, i.e. 2.0 ppm to the low field, the absorption at δ = 6.13 ppm is assigned to CpV while the absorption at δ = 5.75 ppm is assigned to CpCr. Again keeping in mind a valence-electron-induced shift of 1 ppm—in this case for the CpCr unit—the intrinsic charge-induced shift for CpCr comes to 0.46 ppm. In this case no valence-electron-induced shift must be considered for CpV because VCr^+ and the reference VV are isoelectronic. Hence, the charge-induced shift for CpV is nearly twice as large as that for CpCr, suggesting a corresponding charge distribution in VCr^+, which is emphasized by the resonance structure A, wherein both of the metal centers present the same valence electron numbers (Chart IV). The resonance structures B and C make contributions to the fact that the Cp ligand in the CpCr unit as well shows a distinct low-field shift. Again a correlation between the charge distribution and the ionization potentials of V and Cr is obvious.

The extraordinary large anisochrony of the different Cp protons of the X-bridged derivatives **1b–d** as well as **2b–d**, showing the resonance signals of the proximal protons low-field shifted by about 2.1 and 3–3.4 ppm with respect to the signals of the distal protons (Figure 18), deserves some comments. In CH_3-, SiR_3-, or GeR_3-substituted mononuclear diagmagnetic cyclopentadienyl metal complexes the chemical shifts of the Cp protons only vary by about 0.2 ppm,[58] and in CH_2- and $SiMe_2$-bridged binuclear Cp compounds without a metal–metal bond theses shift differences only, by way of exception are larger than 0.3 ppm,[58a,59,60] which then are explained by means of addi-

(56) Elschenbroich, Ch.; Gerson, F. *J. Am. Chem. Soc.* **1975**, *97*, 3556.

(57) Moore, C. E. Analysis of Optical Spectra, NSRDS-NBS 34, Office of Standard Reference Data, National Bureau of Standards, Washington, D.C.

(58) (a) Abel, E. W.; Moorhouse, S. *J. Organomet. Chem.* **1971**, *29*, 227. (b) Köhler, F. H.; Geike, W. A.; Hertkorn, N. *J. Organomet. Chem.* **1987**, *334*, 359.

Table VI. Anisochrony $\Delta\delta_d$ of the Cp Resonance Signals of 1c (X = $SiMe_2$), 2b (X = CH_2), and 2c (X = $SiMe_2$) Originated by the Diamagnetic Anisotropy $\Delta\chi$ of the Metal–Metal Multiple Bond as Well as the Averaged Geometric Factors $[(1 - 3\cos^2\theta)/R]$ of the Cp Protons and $\Delta\chi$ Calculated from Eq 11

	$\Delta\delta_d$, ppm	$10^{27}(1 - 3\cos^2\theta)/R^3$, m^3		$10^{-36}\Delta\chi$,[b] m^3/molecule
		proximal[a]	distal[a]	
1c	1.6	0.84	-9.01	-2270
2b	2.9	2.42	-8.85	-3802
2c	2.6	0.92	-8.35	-3250

[a] Proximal: H(22,25). Distal: H(23,24). [b] SI units.

tional different ligands at the metal center.[60] Therefore only small contributions to the anisochrony of the Cp protons are to be expected due to the electronic effect of the bridging group X.

Larger spreads of Cp resonances normally are observable for the Cp-bridged binuclear complexes with coupled metal atoms wherein the Cp ligands are fixed in a "roof" fashion.[60] Besides a weak influence of X the anisochrony in the cases of **1b–d** and **2b–d** may be essentially due to the diamagnetic anisotropy ($\Delta\chi$) of the metal–metal multiple bond in VV and CrCr.[61]

The effect of an M,M multiple bond on the chemical shift of the ligand protons in binuclear complexes was discussed first by San Filippo[65a] and later famously shown by Cotton and co-workers[65b] as well as by McGlinchey.[65c]

On the basis of McConnels equation $\Delta\sigma = \Delta\chi(1 - 3\cos^2\theta)/12\pi R^3$ [66,67] McGlinchey calculates the diamagnetic anisotropy ($\Delta\chi$) of a metal–metal multiple bond from the shift difference ($\Delta\delta_d$) of two suitable protons, H_1 and H_2, incorporated in this dinuclear complex.[65c]

$$\Delta\delta_d = \Delta\sigma_1 - \Delta\sigma_2 = \frac{\Delta\chi}{12\pi}\left(\frac{1 - 3\cos^2\theta_1}{R_1^3} - \frac{1 - 3\cos^2\theta_2}{R_2^3}\right) \quad (11)$$

The experimental $\Delta\delta_d$ values of **1c**, **2b**, and **2c** are obtained by subtracting other shielding effects mentioned in ref 61 from the spectroscopic shift differences (Table VI).

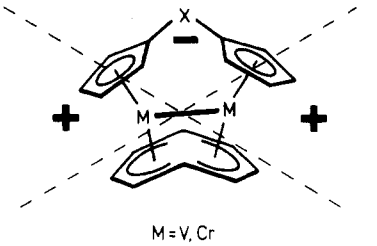

Figure 19. Shielding (+) and deshielding (−) areas in synfacial $X(Cp'M)_2(\mu\text{-Cot})$ complexes (M = V, Cr).

Since the molecular structures of **1c** and **2c** show two different R and θ values for H(22,25) as well as H(23,24) (see ref 5), which are equilibrated in solution by a wagging motion of the bridging group X, the average of the geometric factors of the positions 22 and 25 and positions 23 and 24 is required for eq 11.

With regard to the averaged geometric factors R and θ calculated from the structural data (Table VI) for **2c** we obtain $\Delta\chi$ on the order of -3250×10^{-36} m^3/molecule for CrCr; on the basis of the structure of **1c** $\Delta\chi$(VV) amounts to -2270×10^{-36} m^3/molecule.[68] Taking the averaged geometric factors of the structure of **2b** and the calculated $\Delta\chi$(CrCr), the estimated anisochrony in **2b** enlarges to $\Delta\delta_d$ = 2.9 ppm, which is in excellent agreement with the experimental value proposed.

With these $\Delta\chi$ values the pronounced low-field shifts of the Cp-bridging groups especially CH_2 in VV and CrCr are easily understood. If we assume similar geometric factors in **1b** and **2b**, the low-field shift induced by $\Delta\chi$ is $\Delta\sigma$ = 1.3 ppm for the CH_2 group in **1b**, which seems reasonable with respect to the shift differences between the CH_2 and Cp protons in other CH_2-bridged binuclear Cp complexes with or without a metal–metal single bond.[60] The low-field shift of the CH_2 protons in **2b** calculated from McConnel's equation with $\Delta\chi$ of **2c** is somewhat larger ($\Delta\sigma$ = 1.9 ppm) although these protons on the whole are more shielded than in **1b**, which is due to the different valence-electron-induced shifts of VV and CrCr.

In analogy the deshielding $\Delta\sigma$ of the $SiMe_2$ group in **1c** can be calculated to 0.53 ppm, which agrees well with the difference between the observed shift of the free ligand $Li_2(Cp_2SiMe_2)$ (δ_{SiMe_2} = 0.33 ppm) and the complex **1c** (δ_{SiMe_2} = 0.92 ppm).[70] At this stage it must be mentioned clearly that our approach to estimate $\Delta\chi$ can be understood only in a coarse quantitative way because of the assumptions made above. But nevertheless with a degree of

(59) It must be noted that the assignment of the ^{1}H(Cp) resonance signals to the different positions are only done in ref 58b, wherein the more low-field shifted resonances are allocated to the Cp protons distal to the Si and Ge substituents, which means an anisochrony contrary to our findings.

(60) (a) Werner, H.; Scholz, H. J.; Zolk, R. *Chem. Ber.* **1985**, *118*, 4531. (b) Bitterwolf, T. E. *J. Organomet. Chem.* **1986**, *312*, 197. (c) Wegner, P. A.; Uski, V. A.; Kiester, R. P.; Dabestani, S.; Day, V. W. *J. Am. Chem. Soc.* **1977**, *99*, 4846. (d) Day, V. W.; Thompson, M. R.; Nelson, G. O.; Wright, M. E. *Organometallics* **1983**, *2*, 494. (e) Abriel, W.; Heck, J. *J. Organomet. Chem.* **1986**, *302*, 363. (f) Baumann, R.; Malisch, W. *J. Organomet. Chem.* **1986**, *303*, C33. (g) Heck, J. *J. Organomet. Chem.* **1986**, *311*, C5.

(61) An estimation of the shielding effects caused by (i) the ring current anisotropy of the adjacent Cp ligands[62] and (ii) the anisotropy of the η^3-allylic bonds of the distal C_3 units (C12–14, C16–18)[63,64] on the proximal and distal protons H22,25 and H23,24, respectively, results in a shielding of the latter relative to the former by 0.5 ppm at the most.

(62) (a) Mayo, R. E.; Goldstein, J. H. *J. Mol. Phys.* **1966**, *10*, 301. (b) Kamezawa, N. *J. Magn. Reson.* **1972**, *11*, 88.

(63) Haigh, C. W.; Mallion, R. B. *Org. Magn. Reson.* **1972**, *4*, 203.

(64) Note that the C,C bonds in this C_3 part are distinctly shorter than the C,C distances from C12,14 to the bridging carbons C11,15 (138 and 146 pm, respectively, in 1c and 141 and 145 pm, respectively, in **2b**) (see also ref 2a, 3a, and 5).

(65) (a) San Filippo, J., Jr. *Inorg. Chem.* **1972**, *11*, 3140. (b) Agaskar, P. A.; Cotton, F. A. *Polyhedron* **1986**, *5*, 899. (c) McGlinchey, M. J. *Inorg. Chem.* **1980**, *19*, 1392.

(66) McConnell, H. M. *J. Chem. Phys.* **1957**, *27*, 226.

(67) R is the distance from the center Z of the M,M bond to the proton under study. The angle θ is located between the vector **R** and the M,M bond. $\Delta\sigma$ is given in ppm, R in nm and $\Delta\chi$ in SI units m^3/molecule, $\Delta\chi = \chi_\parallel - \chi_\perp$ and ($\chi_\parallel$ and $\chi_\perp$ are the mean values of the diamagnetic susceptibilities).

(68) Although in a strict sense eq 11 is only fulfilled for an axially symmetrical M,M multiple bond,[69] nevertheless we made an attempt for an approximate evaluation of $\Delta\chi$ of the μ-Cot complexes using the modified form in eq 11. Because of the molecular symmetry as well as the nature of the M,M multiple bond in VV (σ^2, π^2, δ^2) and CrCr (σ^2, π^2, δ^2, δ^{*2}), three diamagnetic susceptibilities, $\chi_{x,y,z}$, strictly speaking should be necessary to describe the diamagnetic anisotropy like it is shown for C,C double bonds, but nevertheless the resulting two different $\Delta\chi$ values of the C,C double bond are very similar (see ref 69). Additionally as mentioned above from the ESR spectra of the doublet radical of $CrCr^{\bullet+}$ an axial **g** tensor is found proving an axial electron distribution around the metal–metal bond in $CrCr^{\bullet+}$. Only in the cases of the radical anions $VV^{\bullet-}$ the **g** tensor and hence the paramagnetic susceptibility deviates from axiality. But, however, for $CrCr^{\bullet-}$ this deviation is still very small. Thus, it seems reasonable to assume an axial metal–metal multiple bond in MM which especially may hold for CrCr.

(69) ApSimon, J. W.; Craig, W. G.; Demarco, P. V.; Mathieson, D. W.; Saunders, L.; Whalley, W. B. *Tetrahedron* **1967**, *23*, 2357.

(70) It must be conceded that $Li_2(Cp_2SiMe_2)$ was measured in [$^2H_8$]-THF whereas 1c was measured in [$^2H_8$]toluene. But nevertheless as can be borrowed from Table V the shifts of the resonance lines of the Me groups in **1d** and **2d** are nearly uneffected by changing the solvent, which is in contrast to the Cp ^{1}H as well as the Cot ^{1}H resonance lines.

certainty the calculated $\Delta\chi$ values above just show the lower limit of the diamagnetic anisotropy of the M,M multiple bond in $(Cp_2M_2)(\mu\text{-Cot})$ (M = V, Cr). The $\Delta\chi$ values are in the order of magnitude of those values derived by McGlinchey and co-workers for other metal–metal multiple bonds.[65c] The obtained $\Delta\chi$ values of the Cp-bridged binuclear μ-Cot complexes VV and CrCr permit us to explain the distinct low-field shift of the protons in the bridging position of the Cp ligand in relation to other bridged binuclear Cp complexes. Thus, irrespective of the exact quantity of $\Delta\chi$ for the M,M multiple bond in VV and CrCr the periphery of the CpM part has to be divided into a deshielding area (−), proximal to the M,M bond, and a shielding area (+), distal to it (Figure 19). Considering the Cr,Cr double bond in CrCr this result stands in marked contrast to the shielding regions of C,C double bonds, where the protons at the end of the C,C bonding are deshielded and the protons in the nodal plane of the C,C double bond as well as above it are shielded.[69] The M,M multiple bonds in VV as well as in CrCr obviously behave more like a C,C triple bond or M,M triple and quadruple bonds, suggesting a decisive influence of the nature of the AO's forming the metal–metal multiple bond. Surprisingly the diamagnetic anisotropy enlarges on going from VV to CrCr although the formal bond order decreases. This fact points out the importance of non- or antibonding electrons on the metal centers for the diamagnetic anisotropy.

The application of the approximately estimated value of $\Delta\chi$ on the shift of the Cot protons in the homobinuclear μ-Cot complexes is much more difficult or almost impossible because from the molecular structure it becomes clear that the metal–carbon and carbon–carbon bond lengths as well as the corresponding bond angles in the M_2-μ-Cot unit differ distinctly from each other, being in sharp contrast to the CpM unit (Table V).[2,3,5] Therefore the proton shifts of the complexed Cot ligand ought to be dominated by the different bonding characteristics of the various metal–carbon bonds. This best can be compared to the η^3-allyl and η^5-pentadienyl complexes.[71,72]

Despite this imponderability from the qualitative picture of the cone of the anisotropy, it can be shown that the two planes of the η^5 units of the Cot ligand may be almost parallel and near the border line of the cone. Therefore the effect of the anisotropy on the chemical shift of the Cot protons should be expected to be feeble.

However, it would be desirable to get more information about the diamagnetic anisotropy of the metal–metal bonds showing the dependence from the bond order, the nature of the metal orbitals forming the M,M bond, and the number of nonbonding metal d electrons.

As additional evidence for a metal–metal multiple bond in the VV complexes, we take the unusual low-field shift of the ^{51}V NMR signals (Table IV); normally the ^{51}V absorptions of organovanadium compounds are observed distinctly high field from $VOCl_3$.[26] Considerable low-field shifts of metal NMR signals are found for compounds wherein metal–metal multiple bonds have to be considered as in $[CpMo(CO)_2]_2$ or dimeric molybdenum carboxylato complexes.[73] The NMR shielding constant σ of the metal nuclei is dominated by the paramagnetic term $\sigma_{para} = -\text{const}\langle\gamma^{-3}\rangle k'^2\Delta E^{-1}$ (see also ref 26), where ΔE is the average over the transition between the ground state and all excited states. Because the energy differences ΔE of the MO of the metal multiple bonds are in most cases small, this could give rise to extreme low-field shifts.

Chart V

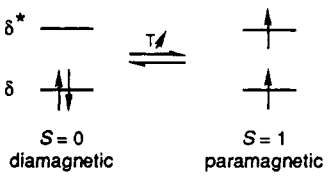

The most striking feature of the NMR spectra is the difference in the temperature dependence of VV and CrCr: whereas the chemical shifts of the signals of CrCr are almost temperature independent and only for the Cot ligand a line broadening is noted below T = 240 K, the resonance signals of VV are low-field shifted and the line widths increase significantly with growing temperature (Figure 18). Additionally, some of the ^{13}C signals of VV get broader and finally are cancelled in some cases upon warming (Figure 12). This unexpected temperature-dependent characteristics of the NMR spectra of the Cot-bridged binuclear vanadium complexes **1a–d** are attributed to a singlet–triplet equilibrium. That means that the energy of the LUMO is positioned close enough to the HOMO to be populated thermally (Chart V), which is in agreement with the conception of a weak δ interaction in VV (Figure 17, vide supra), with

$$-RT \ln K = \Delta G \tag{12}$$

and

$$\Delta G = \Delta H - T\Delta S \tag{13}$$

where K is the constant of the singlet–triplet equilibrium and ΔG the corresponding molar free enthalpy change.

The first intensive work on singlet–triplet equlibrium studied via ^1H NMR was carried out in the area of the planar–tetrahedral equilibrium of Ni(II) complexes in solutions.[74] This is in marked contrast to the organometallic chemistry, where only few compounds are known showing high spin–low spin equilibria studied by NMR methods,[75] in particular organometallic compounds wherein metal–metal single or multiple bonds must be considered.[75g]

The observed chemical shift of a nucleus i (δ_i) in a system with a singlet–triplet equilibrium is given by the contributions of a paramagnetic term, $\delta_{i,para}$ (eq 15), and a diamagnetic term, $\delta_{i,dia}$[74,76–78] where

$$\delta_{i,para} = \frac{C_i}{T}[1 + \exp(\Delta G/RT)]^{-1} \tag{14}$$

(71) Chisholm, M. H.; Godleski, S. *Prog. Inorg. Chem.* **1976**, *20*, 299 and references therein.
(72) Wilson, D. R.; Ernst, R. D.; Cymbaluk, T. H. *Organometallics* **1983**, *2*, 1220.
(73) Minelli, M.; Enemark, J. H.; Brownlee, R. T. C.; O'Connor, M. J.; Wedd. A. G. *Coord. Chem. Rev.* **1985**, *68*, 169.

(74) (a) Eaton, D. R.; Philipps, W. D. *Adv. Magn. Reson.* **1965**, *1*, 103 ff and references cited therein. (b) Holm, R. H.; Hawkins, C. J. In *NMR of paramagnetic Molecules. Principles and Applications*; (LaMar, G. N., Horrocks, W. DeW., Jr.; Hom, R. H., Eds.; Academic Press: New York, 1973; p 243 ff and references cited therein.
(75) (a) Gütlich, P.; McGarvey, B. R.; Kläui, W. *Inorg. Chem.* **1980**, *19*, 3704. (b) Köhler, F. H.; Doll, K. H.; Prössdorf, W.; Müller, J. *Angew. Chem.* **1982**, *94*, 145. (c) Klein, H.-F.; Fabry, L.; Witty, H.; Schubert, K.; Lueken, H.; Stamm, U., *Inorg. Chem.* **1985**, *24*, 683. (d) Werner, H.; Ulrich, B.; Schubert, U.; Hofmann, P.; Zimmer-Gasser, B. *J. Organomet. Chem.* **1985**, *297*, 27. (e) Lemenovskii, D. A.; Urazowski, I. F.; Grishin, Yu. K.; Roznyatovsky, V. A. *J. Organomet. Chem.* **1985**, *290*, 301. (f) Olson, W. L.; Stacy, A. M.; Dahl, L. F., *J. Am. Chem. Soc.* **1986**, *108*, 7646. (g) Heck, J.; Rist, G. *J. Organomet. Chem.* **1988**, *342*, 45.
(76) According to the common notation in NMR spectroscopy shifts to a lower magnetic field are defined as positive; the negative sign of the original equation was omitted (see ref 65b, 69). Within this definition a positive spin density on the observed nuclei ($a_i > 0$) still causes a low-field shift whereas $a_i < 0$ causes a high-field shift.
(77) Horrocks, W. D., Jr. *J. Am. Chem. Soc.* **1965**, *87*, 3779.

and

$$C_i = a_i \frac{\gamma_e}{\gamma_h} \frac{g\beta S(S+1)}{6SK} \qquad (15)$$

It has to be mentioned that a handicap of this method is the temperature dependence of the diamagnetic shift $\delta_{i,dia}$, which particularly matters if the induced paramagnetic shift $\delta_{i,para}$ is smaller than 1 ppm within the employed temperature range as it is observed for VV. This delimma can be restricted by introducing an appropriate internal diamagnetic standard, which in our cases are the analogue Cr complexes.

For a clear-cut solution of eq 14 it would be necessary to know either the hfcc a_i or ΔG if we assumed $g_{iso} = 2.0$, consistent with the g_{iso} value of the doublet species $VV^{\bullet-}$. But both of these parameters unfortunately cannot be obtained experimentally; hence we are induced to ascertain the energetic parameters as well as C_i from the least-squares adjustment.

In Figure 20 the temperature dependence of δ_i of the Cp protons is depicted for **1a–d** as well as the least-squares fits from eq 14 (solid lines). Because of the substantial line width at high temperature, the chemical shifts of the proximal Cp protons were taken to $T = 380$ K only while for the distal protons the chemical shifts were taken to $T = 400$ K. The value for ΔH, ΔS, C_i, and δ_{dia} in Table VII were obtained without further restriction and independently from each other in the cases of the two different Cp protons in **1b–d**. As can be taken from Figure 20 the experimental values of δ_i fit the theoretical curves very well, and the goodness of fit is seen by the standard deviation

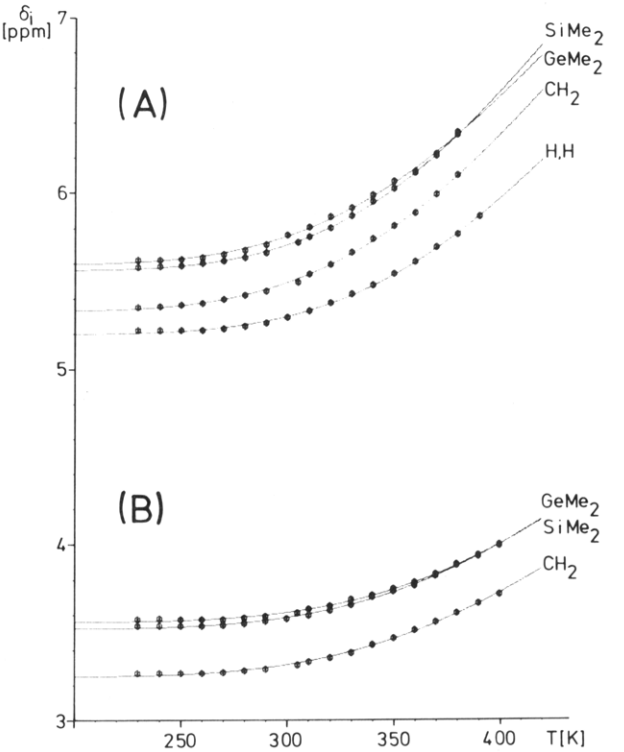

Figure 20. Temperature-dependent ^1H NMR shifts (δ) of the Cp protons H(22,25) (A) and H(23,24) (B) of **1b–d** as well as δ_i(Cp) of **1a** (denoted as H,H). The solid curves have been obtained from adjusting eq 14 and 15 with the use of the parameters listed in Table VII.

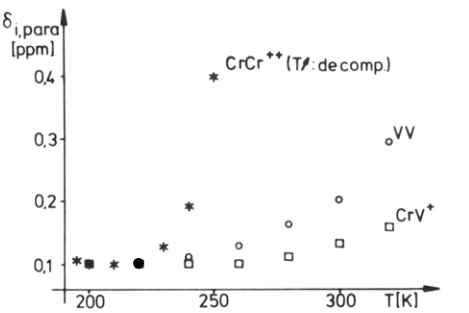

Figure 21. Temperature-dependent, paramagnetic-induced shift ($\delta_{i,para}$) of the Cp protons in **1a** (VV), $\mathbf{2d}^{2+}$ ($CrCr^{2+}$), and $\mathbf{3}^{+}$ (VCr^{+}).

s, which shows that the experimental δ_i values deviate from the theory by less than 0.01 ppm mostly.

The ΔH values derived from the least-squares adjustment of the chemical shift of the distal protons generally are about 5–10% larger than the ΔH values obtained for the proximal protons. This effect may be due to the smaller temperature dependence of the paramagnetic-induced shift of the distal protons, which make up only half of the shift range of the proximal protons within the same temperature range. Hence, systematical errors become more important for δ_i of H(23,24), and the more reliable results should be gathered from the shifts of H(22,25). But nevertheless the ΔH as well as the ΔS values for the different kinds of protons in the Cp-bridged derivatives are still in quite good consistency and confirm our model of a diamagnetic–paramagnetic equilibrium in VV.

The differences in C_i must be attributed to the different ^1H hfcc a_i reflecting the various chemical environments of the Cp protons. The positive value of ΔH confirms the singlet state as the ground state in solution, and its magnitude is in the order of other polynuclear organometallic complexes showing such a singlet–triplet equilibrium

(78) a_i means the isotropic hfcc of the ith nucleus (here proton) γ_e and γ_H are the magnetogyric ratios of the electron and proton, respectively, g represents the isotropic g value and S the spin state of the paramagnetic form, β is the Bohr magneton, and k is the Boltzmann factor. The diamagnetic term $\delta_{i,dia}$ can be obtained from low-temperature spectra. The paramagnetic term (eq 14) only includes the contact shift, whereas the dipolar shift is neglected[74] which depends on a geometric factor $(1-3\cos^2\theta/R^3)$ (θ is the angle between a line joining the paramagnetic center and the proton—vide supra (eq 11)—and the principle axis of the molecule; R is the distance between the paramagnetic center and the proton under study) and the anisotropy of the **g** tensor. In the complexes under consideration we assume a close electronic relation between the triplet state containing single population of the δ as well as δ^* orbitals and the doublet state in which the δ^* MO as well is populated by a single electron, but an electron pair is filled into the bonding δ-type orbital (Figure 17 and Chart V). Because of the small g anisotropy of the 29 ve species (Table III), it is obvious that the g anisotropy in the triplet state would be small as well and the influence of the dipolar interaction on the paramagnetic shift should be of no significance. The application of eq 14 also presumes that the measured isotropic shifts are averaged over the diamagnetic and paramagnetic isomers: this is suggested from the temperature dependence of the proton shifts of VV. If the singlet–triplet interconversion was slow compared to the NMR time scale, first the temperature dependence of the chemical shifts of VV would be as feeble as for the diamagnetic CrCr complexes and second the Me resonance signals for the $SiMe_2$-bridged as well as for the $GeMe_2$-bridged triplet isomers ought to be expected in the range of ±10 ppm relative TMS.[79] As a third condition Curie's law must be warranted for the triplet isomer, which normally can be checked by temperature-dependent studies on the susceptibility of the pure triplet isomer. But the pure paramagnetic isomer of VV cannot be achieved at temperatures above $T = 450$ K because of its decomposition. However, from the results of mononuclear sandwich compounds there are good reasons to assume Curie behavior in the range of $T = 200$–400 K.[75,80]

(79) The Me-proton resonance line of the $SiMe_2$ and $GeMe_2$ doubly bridged vanadocenophanes $(CP_2X)_2V_2$ with six (!) unpaired electrons, which could be isolated as byproducts in the synthesis of **1c** and **1d**, are located at $\delta(340\text{ K}) = 13.6$ ppm and $\delta(340\text{ K}) = 8.6$ ppm, respectively.[5] The $SiMe_3$-substituted mononuclear vanadocene with three unpaired electrons shows a singlet at $\delta(320\text{ K}) = +9.2$ ppm (low field from TMS) (see: Köhler, F. H.; Geike, W. A. *J. Organomet. Chem.* **1987**, *328*, 35).

(80) (a) Rettig, M. F. In *NMR of Paramagnetic Molecules. Principles and Applications*; LaMar, G. N., Horrocks, W. Dew., Jr., Holm, R. H., Eds.; Academic Press: New York, 1973; p 217 ff. (b) Warren, K. D. *Inorg. Chem.* **1974**, *13*, 1317 and references cited therein. (c) For special cases of non-Curie behavior of metallocenes in solution see also: Nebedanz, N.; Köhler, F. H.; Müller, G.; Riede, J. *J. Am. Chem. Soc.* **1986**, *108*, 3281.

Table VII. Fit Parameters (ΔH, ΔS, C_i, δ_{dia}, s)[a] from the Least-Squares Adjustment of Eq 14 to the Temperature Dependence of the Cp ^{1}H NMR Shifts[b] of the 28 ve Species $[X(Cp'_2MM')(\mu\text{-Cot})]^{n+}$

compounds			Cp position	ΔH, kJ mol^{-1}	ΔS, J mol^{-1} K^{-1}	C_i, K	δ_{dia}, ppm	$10^3 s$, ppm
$n = 0$	M = M′ = V	X = H,H (**1a**)		23.8	42.8	2630	5.19	7.94
		X = CH_2 (**1b**)	distal	22.8	37.8	2270	3.25	7.07
			proximal	21.9	37.0	3490	5.33	6.69
		X = $SiMe_2$ (**1c**)	distal	24.1	43.7	2560	3.56	5.54
			proximal	23.4	38.7	2890	5.56	6.74
		X = $GeMe_2$ (**1d**)	distal	23.5	38.7	2360	3.52	8.20
			proximal	21.6	37.0	3110	5.59	11.7
$n = 1$	M = V, M′ = Cr	X = H,H (**3**$^+$)		26.9[c,d]			5.74	
				25.6[c,e]			6.12	
$n = 2$	M = M′ = Cr	X = $GeMe_2$ (**2d**$^{2+}$)	distal	~15[f]			3.69	

[a] s = standard deviation = $(SLS/n - 1)^{1/2}$ where SLS = sum of least squares and n = number of measurements at different temperatures. [b] The temperature was changed from 230 to 400 K in steps of 10 °C. [c] Calculated from $\Delta\delta_{i,para}$ (**1a**)/$\Delta\delta_{i,para}$ (**3**$^+$) = $\{1 + \exp[\Delta G(\mathbf{3}^+)/RT]\}/\{1 + \exp[\Delta G(\mathbf{1a})/RT]\}$ in a given temperature range (200–320 K) assuming ΔS and C_i are of equal for **1a** and **3**$^+$. [d] Based on the paramagnetic-induced shift of the CpCr unit in **3**$^+$. [e] Based ont he paramagnetic-induced shift of the CpV unit in **3**$^+$. [f] Calculated for the distal protons H(23,24) in **2d**$^{2+}$ in accordance to footnote *c*: $\Delta\delta(\mathbf{1d}_{distal})_{para}/\Delta\delta(\mathbf{2d}^{2+}{}_{distal})_{para}$ for $200 \le T \le 250$ K.

without structural change.[75a,f,g]

The change in entropy $\Delta S \approx 40$ J mol^{-1} K^{-1} is considerably larger than is expected from the pure change of the spin state ($\Delta S = R \ln 2S_{high\ spin} + 1)/(2S_{low\ spin} + 1)$).[81] In our case the excited spin state is assumed to be $S_{high\ spin} = 1$ and hence $\Delta S = 9.13$ J mol^{-1} K^{-1}. As mentioned previously the excess of the entropy obtained from the experiment should be attributed to an increase of the intramolecular vibrational degrees of freedom in the excited state.[81] A 3–5-fold excess of ΔS compared to the theoretical value is observed in most cases.[74,75]

As it was possible to prepare two further 28 ve species, i.e. VCr^+ (**3**$^+$) and $CrCr^{2+}$ (**2d**$^{2+}$), we studied the temperature dependence of their chemical shifts as well. Figure 21 shows their paramagnetic shifts as a function of T in comparison to VV. For $CrCr^{2+}$ the shifts of the distal protons H(23,24) were taken because of the broad line width of the absorption signals of the proximal protons H(22,25). But unfortunately the dication decomposes completely at $T > 250$ K in a few minutes, and therefore its paramagnetic-induced shift could just be studied in a very small temperature range. On the other side the shift range of VCr^+ from 200 to 320 K is too small to get a satisfying least-squares fit. But nevertheless, with the assumption of the same $a(^1H)$ hfcc in VV, VCr^+, and $CrCr^{2+}$ and an equal entropy change ΔS, ΔH of VCr^+ and $CrCr^{2+}$ can be estimated (Table VII) from the paramagnetic-induced shift $\delta_{i,para}$ at a given temperature. These values show a decreasing singlet–triplet separation in the series $VCr^+ > VV > CrCr^{2+}$, which can be understood by the contraction of the MO in $CrCr^{2+}$ compared to that in VV upon the positive charge in the Cr dication. This results in less overlap of the $1a_1$ orbitals for the δ interaction (Figure 17). Consequently the thermal population of the δ^* MO becomes easier, which is expressed by the decrease in ΔH. The larger singlet–triplet separation in VCr^+ must be attributed to the different energy levels of the individual metal centers resulting in a stronger δ,δ^* splitting as implied qualitatively in Figure 17.

From eq 12 and 13 the constant K of the singlet–triplet equilibrium in VV can be calculated and hence the amount of triplet species in solution: at $T = 300$ K the amount of VV(triplet) is about 1% of VV(singlet) and at $T = 200$ K even smaller than 10^{-2}%. These values demonstrate that the ^{1}H NMR spectroscopy is a powerful tool for the investigation of diamagnetic–paramagnetic equilibria because of its sensitivity. Another advantage of this method is that the measured chemical shifts are intrinsic effects of the paramagnetism of the molecules in contrast to the bulk susceptibility measurements with which the paramagnetism of the whole sample is measured including the paramagnetic impurities. This in particular will raise great problems if the amount of the paramagnetic form is very small, e.g. <1%, and the substances under study are highly sensitive against oxygen, which easily leads to a drag in of paramagnetic impurities.

(81) Gütlich, P. *Struct. Bonding (Berlin)* **1981**, *44*, 83.

Conclusions

The extensive and manifold investigations of the different electron-poor μ-Cot complexes **1–3** prove a distinct metal–metal interaction as shown by (i) the well-separated electrochemically reversible redox pairs ($\Delta E° > 1000$ mV) coupled with one-electron transfers, (ii) the delocalized nature of the unpaired electron in the homobinuclear radical ions with 29 as well as 31 ve, (iii) the pronounced diamagnetic anisotropy ($\Delta\chi$) of the dimetal unit leading to a strong anisochrony of the Cp protons in the Cp-linked complexes, and (iv) the unusual low-field shift of the ^{51}V resonance signals of the VV derivatives. On the other hand, there are some characteristics indicating only a weak δ interaction of the metal–metal bond in these kind of complexes: (i) the predominant localization of the unpaired electron in VCr on the vanadium center, (ii) the poor balance of charge in VCr^- and VCr^+, and (iii) the thermally excited triplet state of the 28 ve species. The metal–metal interaction of heterobinuclear electron-poor ($\sum$ve < 34) μ-cyclopolyolefin complexes particularly is the topic of our current work.

Acknowledgment. This work was supported by the Deutsche Forschungsgemeinschaft, and we are greatly indebted to the BASF for the donation of Cot. We are also very much obliged to Prof. Dr. D. Rehder for doing the ^{51}V NMR measurements.

Registry No. **1a**, 107201-40-1; **1a**$^-$, 85234-88-4; **1b**, 122357-73-7; **16**$^-$, 122382-41-6; **1c**, 122357-74-8; **1c**$^-$, 122357-80-6; **1d**, 122357-75-9; **1d**$^-$, 122357-81-7; **2a**, 85116-51-4; **2a**PF_6, 122357-92-0; **2a**$^+$, 122357-82-8; **2a**$^-$, 122357-86-2; **2b**, 122357-76-0; **26**$^+$, 122357-83-9; **26**$^-$, 122357-87-3; **2c**, 122357-77-1; **2c**$^+$, 122357-84-0; **2c**$^-$, 122357-88-4; **2d**, 122357-78-2; **2d**$^+$, 122357-85-1; **2d**$^-$, 122357-89-5; **2d**$^{2+}$, 122357-90-8; **3**, 122357-79-3; **3**PF_6, 122357-93-1; **3**$^+$, 122357-91-9; **3**$^-$, 122382-42-7; **4**, 57002-78-5; **5**, 122357-94-2; $(FeCp_2)PF_6$, 11077-24-0.